EURONU WP6 2009 yearly report: Update of the physics potential of Nufact, superbeams and betabeams

Contributors: J. Bernabeu[a], M. Blennow[b], P. Coloma[c], A. Donini[a,c],
C. Espinoza[a], E. Fernández-Martinez[b], P. Hernández[a], P. Huber[d],
J. Kopp[e], A. Longhin[f], J. López-Pavón[c], M. Mezzetto[g], T. Ota[h],
T. Schwetz[i] and W. Winter[h]

[a] *Dep. de Física Teórica and IFIC, Universidad de Valencia and CSIC,
Apart. 22085, 46071 Valencia*
[b] *Max-Planck-Insitute Für Physik, Föhringer Ring,
80805 München, Germany*
[c] *Dep. de Física Teórica and Instituto de Física Teórica, UAM-CSIC,
Cantoblanco, 28049 Madrid, Spain.*
[d] *Department of Physics, IPNAS, Virginia Tech, Blacksburg,
Virginia, VA 24061, USA.*
[e] *Theoretical Physics Department, Fermilab, P. O. Box 500,
Batavia, IL60510 USA.*
[f] *Commissariat à l'Energie Atomique (CEA), Dir. des Sciences de la Matière,
25 Rue Leblanc, Paris 75015, France*
[g] *INFN, Sezione di Padova, Via Marzolo 8,
35131 Padova, Italy.*
[h] *Institute Für Theoretische Physik und Astrophysik, Universität Würzburg,
97074 Würzburg, Germany.*
[i] *Max-Planck-Institute Für Physik, P.O. Box 103980,
69029 Heidelberg, Germany*

December 24, 2012

EURONU-WP6-10-19

1

1   Neutrino masses and new physics

The main motivation of a future neutrino physics programme is to understand what the new physics associated to neutrino masses is. We know for sure that new degrees of freedom must be added to the Standard Model (e.g. right-handed neutrinos) at some energy scale Λ. If Λ is much larger than the electroweak scale, there is a natural explanation of why neutrinos are so light. Indeed the effects of *any* such new physics must be generically well described at low energies by an effective Lagrangian which contains the Standard Model, plus a tower of higher dimensional operators constructed with the SM fields and satisfying all the gauge symmetries:

$$\mathcal{L} = \mathcal{L}_{SM} + \sum_i \frac{\alpha_i}{\Lambda} \mathcal{O}_i^{d=5} + \sum_i \frac{\beta_i}{\Lambda^2} \mathcal{O}_i^{d=6} + ... \tag{1}$$

The effective operators, $\mathcal{O}_i$, are ordered by their mass dimension, since the higher the dimension, the higher the power of Λ that suppresses them. The dominant operator is therefore the lowest dimensional one, with $d = 5$, which is precisely the Weinberg's operator:

$$\mathcal{O}^{d=5} = \bar{L}^c \Phi \Phi L, \tag{2}$$

which, as is well known, induces three new ingredients to the minimal SM:

- Neutrino masses

- Lepton mixing

- Lepton number violation

In this context, neutrino masses are very small, because they come from an effective operator which is suppressed by a high energy scale. If we go to operators of $d = 6$, that are suppressed by two powers of Λ, these will generically induce new physics in dipole moments, rare decays, etc. Beyond $d = 6$ we would find operators inducing non-standard neutrino interactions (NSI).

It is also possible that the scale Λ is at or below the electroweak scale, or in other words that neutrino masses are linked to light degrees of freedom, *i.e.* a *hidden* sector which we have not detected yet, because it is weakly interacting. Such scenarios do not offer an explanation of why neutrinos are light, but neutrinos are the natural messengers with such hidden sectors, since they are the only particles in the SM carrying no conserved charge. Such new physics could be related to other fundamental problems in particle physics such as the origin of dark matter and dark energy.
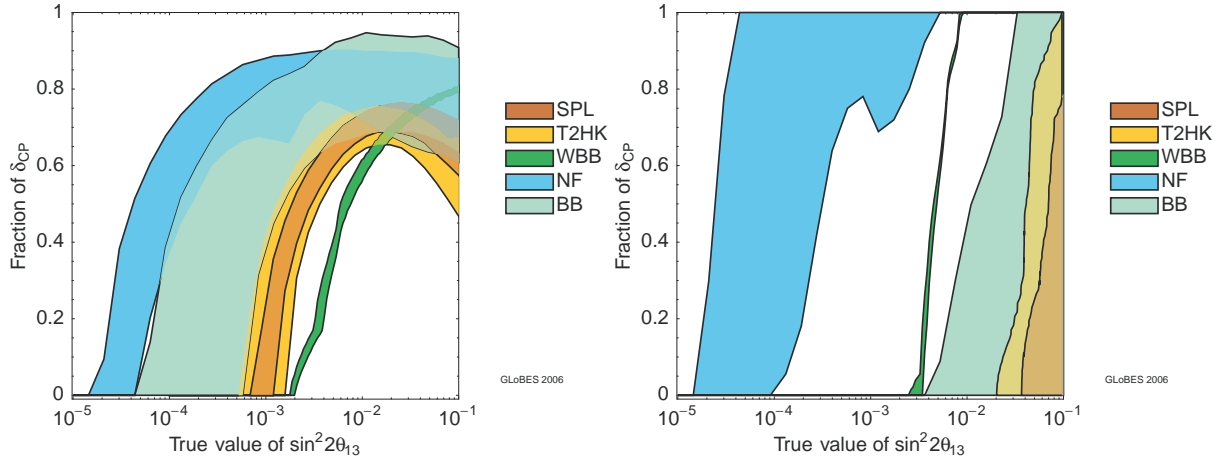
Even though it is not guaranteed that we can fully understand the new physics associated to neutrino masses by measuring them, it is quite clear that we have a good chance to learn something more about it by testing the Standard scenario of 3ν mixing with future and more precise neutrino experiments. In particular we should be able to measure all the fundamental parameters: three mass eigenstates (m_1^2, m_2^2, m_3^2), three angles $(\theta_{12}, \theta_{13}, \theta_{23})$ and one or three CP-violating phases $(\delta, \alpha_1, \alpha_2)$. But, also, it will be very important to search for new physics beyond neutrino masses and mixings, in particular for those effects that are generic in many

models of neutrino masses, such as violations of unitarity, non-standard interactions or the presence of light sterile species. To some extent these searches can also be improved in future facilities and this should be evaluated. Typically such analyses imply dealing with a much larger parameter space, which calls for new tools to perform the fits, in particular Montecarlo methods.

Many studies in the last ten years have shown that we can measure the unknown angle θ_{13}, discover leptonic CP violation and determine the neutrino hierarchy in more precise neutrino oscillation experiments, searching for the subleading channel $\nu_e \leftrightarrow \nu_\mu$ in the atmospheric range. A starting point for the Physics Work Package (WP6) of the EURONU project are the results of the International Scoping Study (ISS) summarized in Figs. 1 [1].

In this first report of WP6 activities the following new results are presented:

- Sect. 2: Re-evaluation of the physics reach of the upcoming generation of experiments to measure θ_{13} and δ (see Ref. [2]).

- Sect. 3: New tools to explore a larger parameter space as needed beyond the standard scenario (see Ref. [3]).

- Sect. 4: Neutrino Factory

  1. Sect. 4.1: evaluation of the physics reach of a Nufact regards sterile neutrinos (see Ref. [4]).
  2. Sect. 4.2: evaluation of the physics reach of a Nufact as regards non-standard interactions (see Ref. [5]).
  3. Sect. 4.3: evaluation of the physics reach of a Nufact as regards violation of unitarity (see Ref. [6]).
  4. Sect. 4.4: critical assessment on long baseline τ-detection at Nufact [7].
  5. Sect. 4.5: new physics searches at a near detector in a Nufact (see Ref. [8]).

- Sect. 5: Beta-beams

  1. Sect. 5.1: choice of ions and location for a $\gamma = 100$ CERN-based β-beam (from [9]).
  2. Sect. 5.2: re-evaluation of atmospheric neutrino background for the $\gamma = 100$ β-beam scenario (from [9]).
  3. Sect. 5.3: study of a two baseline β-beam (see Ref. [10]).
  4. Sect. 5.4: measuring absolute neutrino mass with Beta Beams (see Ref. [11]).
  5. Sect. 5.5: progress on monochromatic β-beams (see Ref. [12]).

- Sect. 6: Update of the physics potential of the SPL super-beam (from [13]).

Figure 1: Comparison of the physics reach of different future facilities in leptonic CP violation (left) and the neutrino mass hierarchy (right). Taken from [1].

2   Up-coming oscillation experiments

The main purpose of the upcoming generation of experiments will be to discover sub-leading effects in neutrino oscillations. This includes the determination of the small lepton mixing angle θ_{13}, establishing CP violation (CPV) in neutrino oscillations for a value of the Dirac CP phase $\delta_{\rm CP} \neq 0, \pi$, and identification of the type of the neutrino mass hierarchy (MH), which can be normal ($\Delta m_{31}^2 > 0$) or inverted ($\Delta m_{31}^2 < 0$). There are several neutrino oscillation experiments currently under construction, which are expected to start data taking soon. These are the reactor neutrino experiments Double Chooz [14], Daya Bay [15], RENO [16] and the accelerator experiments T2K [17] and NOνA [18]. In Ref. [2] the potential of this next generation of experiments towards the three tasks mentioned above has been evaluated. While the primary goal for all of these experiments is the discovery of the yet unknown mixing angle θ_{13}, it might also be interesting to ask the question, whether there is some chance to address also CPV and MH, in case θ_{13} is relatively large. The analysis of Ref. [2] updates previous works [19–23] with respect to the now settled parameters for the considered experiments.

Table 1 summarizes the key parameters of the considered experiments, for further details see [2]. The analysis is performed by using the GLoBES software [24, 25]; the corresponding `glb`-files are available at the GLoBES web-page [24] including detailed technical information on the simulation. In all cases the strategy is to follow as close as possible the original Letters of Intent (LOIs) or Technical Design Reports (TDRs). We have made sure that our sensitivities agree with the "official" curves from the corresponding collaborations under the same assumptions. For the sensitivity analyses we use the oscillation parameter values from Ref. [26]: $\Delta m_{21}^2 = 7.65 \times 10^{-5} \,{\rm eV}^2$, $|\Delta m_{31}^2| = 2.40 \times 10^{-5} \,{\rm eV}^2$, $\sin^2 \theta_{12} = 0.304$, and $\sin^2 \theta_{23} = 0.500$, unless stated otherwise. We impose external 1σ errors on Δm_{21}^2 (3%) and θ_{12} (4%) as conservative estimates for the current measurement errors, as well as Δm_{31}^2 (5%) for reactor experiments if analyzed without beam experiments. In addition, we include a 2% matter density uncertainty.

4

In Ref. [2] various performance indicators have been considered for the nominal configurations of the experiments, such as sensitivity to θ_{13}, potential for large θ_{13}, accuracy to the atmospheric parameters θ_{23}, $|\Delta m_{31}^2|$, CP-violation, and mass hierarchy. In the following we show as an important result the prospective time evolution of the sensitivity to θ_{13}. These calculations are based as much as possible on official statements of the collaborations. Although the assumed schedules and proton beam plans may turn out to be not realistic in some cases, our toy scenario will be illustrative to show the key issues for the individual experiments within the global neutrino oscillation context. The sensitivities are shown as a function of time assuming that data are continously analyzed and results are available immediately.
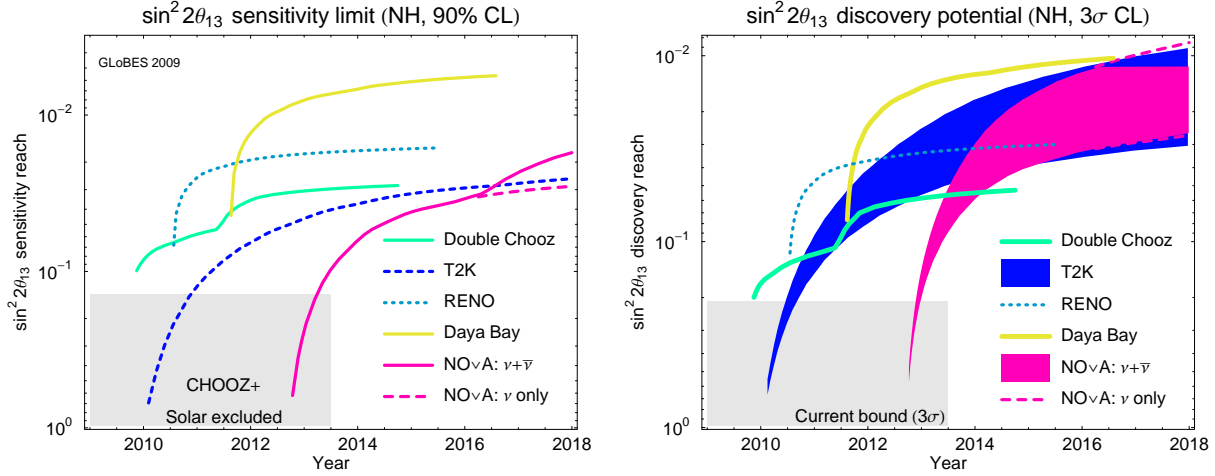
The key assumptions for our toy scenario are as follows. Double Chooz starts late 2009 and runs 1.5 years with far detector only, then with far and near detector. RENO and Daya Bay start mid 2010 and mid 2011, respectively, with all detectors on-line. T2K starts late 2009 with virtually 0 MW beam power, which increases linearly to 0.75 MW reached in 12/2012. From then we assume the full target power of 0.75 MW. The beam runs only with neutrinos. NOνA starts mid 2012 with full beam (0.7 MW), but 2.5 kt detector mass only. Then the detector mass increases linearly to 15 kt in 01/2014. From then we assume the full detector mass of 15 kt. The beam runs with neutrinos first, until the equivalent of three years operation at nominal luminosity (cf., Table 1) is reached, i.e., 03/2016. Then it switches (possibly) to antineutrinos and runs at least until 2019.

We show the θ_{13} sensitivity limit (bound on θ_{13} in case of no signal) as a function of time in Fig. 2 (left). We observe that the global sensitivity limit will be dominated by reactor experiments. As soon as operational, Daya Bay will dominate the global limit. For Daya Bay, time is not critical, but matching the systematics or statistics goals is.[1] If the assumed schedules of both, Double Chooz and Daya Bay are matched, Double Chooz will dominate the θ_{13} sensitivity for about two years in the absence of RENO. If available, RENO, on the other hand, will dominate the θ_{13} sensitivity if it is operational significantly before the end of 2011. As a peculiarity, the θ_{13} sensitivity of NOνA is improved by switching to antineutrinos. However, the global limit will at that time be dominated by the reactor

---

[1]The Daya Bay assumptions of a systematical error of 0.18%, fully uncorrelated among all detectors is more aggressive than for other reactor experiments. For example, if the systematic error is at the level of 0.6% (such as assumed in Double Chooz) and uncorrelated among modules, the Daya Bay sensitivity of $\sin^2 2\theta_{13} = 0.0066$ deteriorates to $\sin^2 2\theta_{13} \simeq 0.01$. If on the other hand the systematic error is 0.38% (the Daya Bay "baseline" value) and assumed to be fully correlated among modules at one site the limit would correspond roughly to the one obtained for an uncorrelated error of $0.38\% \times \sqrt{N} \simeq 0.76\%$ for $N = 4$ modules at the far site. This will lead to a limit of $\sin^2 2\theta_{13} \simeq 0.012$ [27].

Setup	t_ν [yr]	$t_{\bar\nu}$ [yr]	P_{Th} or P_{Target}	L [km]	Detector technology	m_{Det}
Double Chooz	-	3	8.6 GW	1.05	Liquid scintillator	8.3 t
Daya Bay	-	3	17.4 GW	1.7	Liquid scintillator	80 t
RENO	-	3	16.4 GW	1.4	Liquid scintillator	15.4 t
T2K	5	-	0.75 MW	295	Water Cerenkov	22.5 kt
NOνA	3	3	0.7 MW	810	TASD	15 kt

Table 1: Summary of the standard setups at their nominal luminosities.
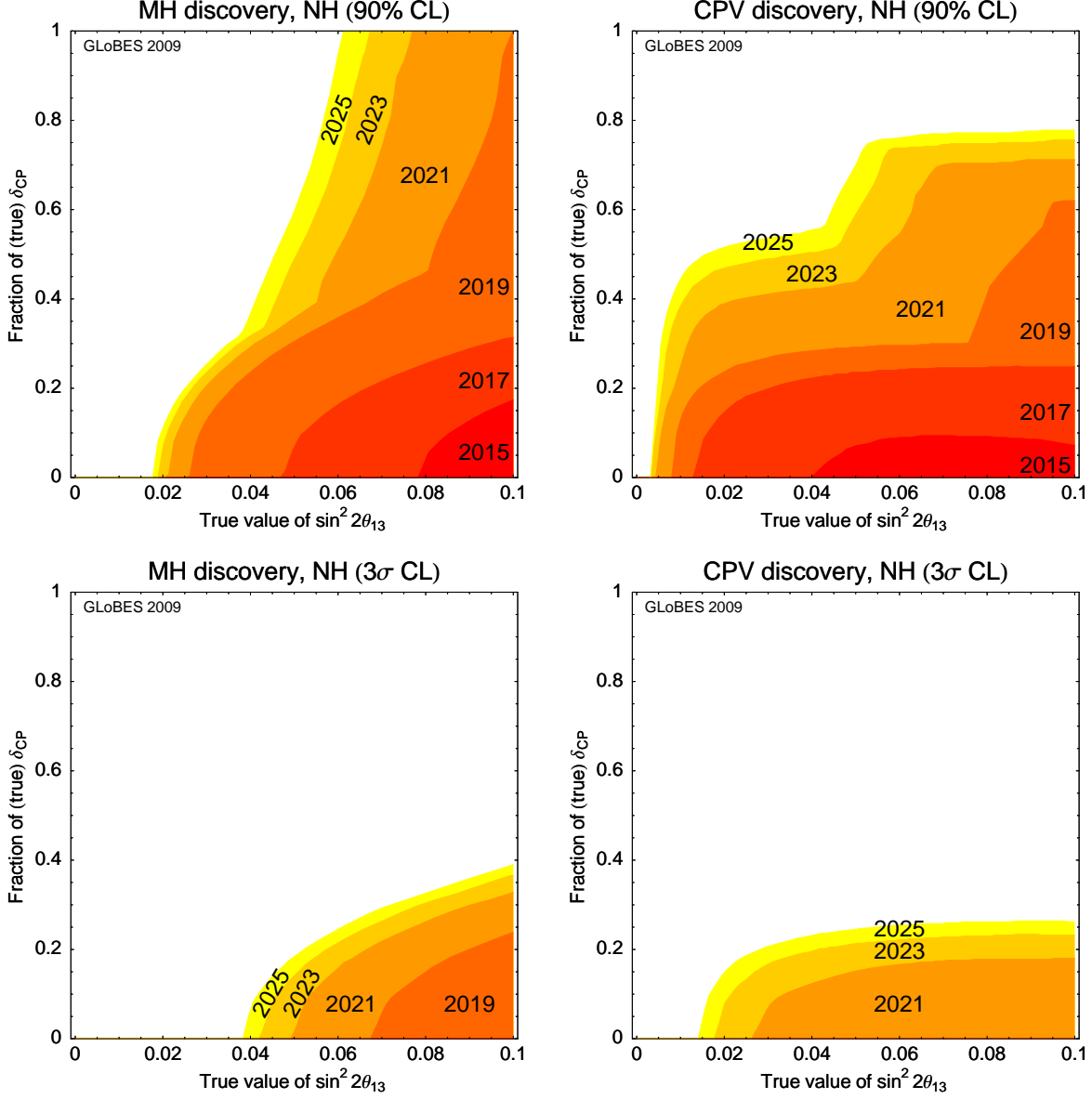
Figure 2: Left: Evolution of the θ_{13} sensitivity limit as a function of time (90% CL), *i.e.*, the 90% CL limit which will be obtained if the true θ_{13} is zero. Right: Evolution of the θ_{13} discovery potential as a function of time (3σ CL), *i.e.*, the smallest value of θ_{13} which can be distinguished from zero at 3σ. The bands reflect the (unknown) true value of δ_{CP}. In both panels we assume normal hierarchy. Taken from Ref. [2].

experiments.

The θ_{13} discovery potential (smallest θ_{13} which can be distinguished from zero) is shown in Fig. 2 (right) as a function of time. For the beam experiments, the dependence on the true value of δ_{CP} is shown as shaded region, whereas the reactor experiments are not affected by the true δ_{CP}. There is a small dependence on the true mass hierarchy for the beam experiments, here we choose a true normal hierarchy. The comparison of the left and right panels in Fig. 2 shows that suitable values of δ_{CP} may significantly improve the discovery potential of beams compared to their sensitivity limit. Indeed, for favorable values of δ_{CP} the discovery reach of beams can be similar to the one of Daya Bay, whereas the sensitivity limit is more like the one from Double Chooz.

If θ_{13} is close to its present bound, and hence will be discovered rather soon, it might be interesting to investigate, whether "modest upgrades" to the proposed setups of T2K and NOνA might allow to address the issues of CP violation and mass hierarchy determination. With "modest upgrades" we mean modifications of existing equipment and infrastructure. This includes a longer running time and an upgraded beam power for both accelerator experiments and the addition of antineutrino running in T2K. To be specific, we assume that a proton driver is installed for T2K, which increases the beam power from 0.75 to 1.66 MW, linearly from 2015 to 2016 [28], and for NOνA we assume a linear increase from 0.7 to 2.3 MW from March 2018 to March 2019 according to "Project X" [29]. We consider these upgraded beams for T2K and NOνA combined with reactor data, and we have performed a global optimization for the switching between neutrinos and antineutrinos in both beams.

Fig. 3 shows the discovery potential as a function of true $\sin^2 2\theta_{13}$ and fraction of true δ_{CP} for times from 2015 to 2025. From the upper row of this figure we conclude that at

Figure 3: Mass hierarchy (left panels) and CP violation (right panels) discovery potentials as a function of true $\sin^2 2\theta_{13}$ and fraction of true δ_{CP} for T2K+NOνA (including beam upgrades and global $\nu/\bar{\nu}$-optimization) and reactor experiments. The upper panels are for 90% CL, the lower panels for 3σ CL. The different shadings corresponds to different points of time. Taken from Ref. [2].

the 90% confidence level, there will be hints for the MH and CPV for $\sin^2 2\theta_{13} \gtrsim 0.05$ for most values of δ_{CP} around 2025. However, certainly a 90% CL is not sufficient to make any meaningful statement about a discovery. Therefore, we show in the lower row of Fig. 3 the corresponding results at 3σ CL. Obviously the sensitivity regions reduce drastically, however, we see from the figure that assuming both beams upgraded, a fully optimized neutrino/antineutrino run plan, and data from reactors a non-negligible discovery potential at 3σ will be reached in 2025. The mass hierarchy can be identified for $\sin^2 2\theta_{13} \gtrsim 0.05$ for about 20% to 40% of δ_{CP} values, whereas CPV can be discovered for $\sin^2 2\theta_{13} \gtrsim 0.02$ for 25% of δ_{CP} values. In both cases, MH and CPV, there is sensitivity for values of δ_{CP} around $3\pi/2$ ($\pi/2$) if the true hierarchy is normal (inverted). This is related to the sign of the matter effect, see, *e.g.*, Ref. [30] for a discussion.

Although "minor upgrades" of existing facilities may provide a non-negligible sensitivity to CP violation and the mass hierarchy, there is high risk associated with this strategy, since for about 75% of all possible values for δ_{CP} no discovery will be possible at the 3σ level. Therefore, we conclude that the upcoming generation of oscillation experiments may lead to interesting indications for the mass hierarchy and CP violation, but it is very likely that an experiment beyond the upcoming superbeams (including reasonable upgrades) will be required to confirm these hints.

3   New tools: MonteCUBES

Many models of new physics that have been discussed in the context of neutrino physics, and in particular long-baseline neutrino oscillation experiments, expand the dimensionality of the neutrino oscillation parameter space. Since the most general standard neutrino oscillation parameter space already includes six free parameters, it is essentially impossible to perform a deterministic analysis of the full parameter space when also including new physics. The common practice has been to fix all of the new physics parameters except for one or two as well as several of the standard oscillation parameters. While this can give a hint at the dependence on the new physics, specific features requiring the interplay of several parameters may be lost. Examples of the new physics are non-standard neutrino interactions (NSI) and non-unitarity of the lepton mixing matrix.

The Monte Carlo Utility Based Experiment Simulator (MonteCUBES) software [3, 31] was introduced to address this issue. The software is a plugin for the General Long Baseline Experiment Simulator (GLoBES) [24, 25] and compiles and installs on computers where GLoBES has already been installed.

3.1   The MonteCUBES plugin

MonteCUBES has been designed to sample the neutrino oscillation parameter space using Markov Chain Monte Carlo (MCMC) mehods, which makes it ideal for studying high-dimensional parameter spaces. We will here give a short introduction to MCMCs before discussing the features included in MonteCUBES.

3.1.1 Markov Chain Monte Carlos

A MCMC is designed to create a representative sample of a probability distribution $P(x)$, where x represents a set of parameters, using stochastic methods. The most common implementation of this is the Metropolis–Hastings algorithm, which is defined as follows:

1. Pick a starting point $\bar{x}$ in parameter space.

2. Using a transition probability function $W(\bar{x} \to x')$, pick a test point x'.

3. Compute the acceptance probability α as

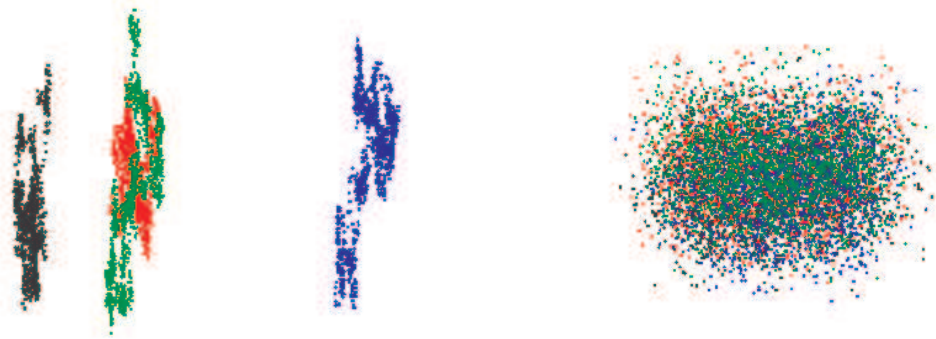$$\alpha = \min \left(1, \frac{P(x')}{P(\bar{x})} \frac{W(x' \to \bar{x})}{W(\bar{x} \to x')} \right).$$

4. Pick a random number r in $[0, 1]$.

5. If $r < \alpha$, then put $\bar{x} = x'$.

6. Add $\bar{x}$ to the list of samples.

7. Repeat steps 2-6 until a sufficiently large number of samples has been produced.

The particular choice of α implies that $P(x)$ is the equilibrium distribution.

The advantage of using a MCMC instead of using deterministic algorithms for exploring large parameter spaces is that, when analyzing an experiment with a high-dimensional parameter space with a classic method, a lot of computer power will be spent on computing χ^2 functions or likelihoods in regions which are not of physical interest. Instead, the MH algorithm is designed to mainly explore the physically interesting region also in high-dimensional parameter spaces (the breaking point where the MH algorithm becomes more suitable is generally around $n = 4$).

In step 7 of the description of the MH algorithm, we have stated that the algorithm should be repeated until a sufficient number of samples has been reached. It is therefore natural to define what is ment by this. Of course, the number of samples must be high enough so that a fairly good approximation of the probability distribution can be reconstructed. However, even though $P(x)$ is the equilibrium distribution, it can take some time to reach this equilibrium. As an example, in Fig. 4, we show four chains that have sampled the same distribution with both bad and good convergence. In the case of bad convergence, the chains are separate, while in the case of good convergence, they all have more or less the same distribution. In MonteCUBES, there are built-in convergence checks, based on running several different MCMCs in parallel and comparing the variance within one chain with the variance in the combined sample (see Ref. [32]). This is done in run-time and the simulations can be run for as long as it takes to converge, or until a maximum number of samples has been reached.

The most straightforward use of MCMCs for experimental analysis is through the use of Bayesian statistics. We use the MCMC to sample the posterior probability distribution

Figure 4: Samples scattered in parameter space for chains with bad (left) and good (right) convergence, respectively. See Ref. [31] for details.

$P(\theta|d)$, where θ is a parameter and d a data set, which according to Bayes' theorem can be written as

$$P(\theta|d) = \frac{P(d|\theta)P(\theta)}{P(d)} \equiv \frac{L_d(\theta)\pi(\theta)}{M}, \tag{3}$$

where $L_d(\theta)$ is the likelihood of getting the data d given the oscillation parameters θ, $\pi(\theta)$ is a prior which summarizes our previous knowledge (or assumptions) on the distribution of θ, and M is a normalization constant.

Once the posterior probability distribution has been sampled, it can be projected onto any subspace of the parameters by simply ignoring the values of other parameters. The Bayesian regions of the p most likely parameter values are then defined as the smallest regions containing the probability p. Note that this differs from the frequentist confidence regions at level p, which are the regions of parameter space such that the actual experimental outcome is among the p less extreme outcomes[2].
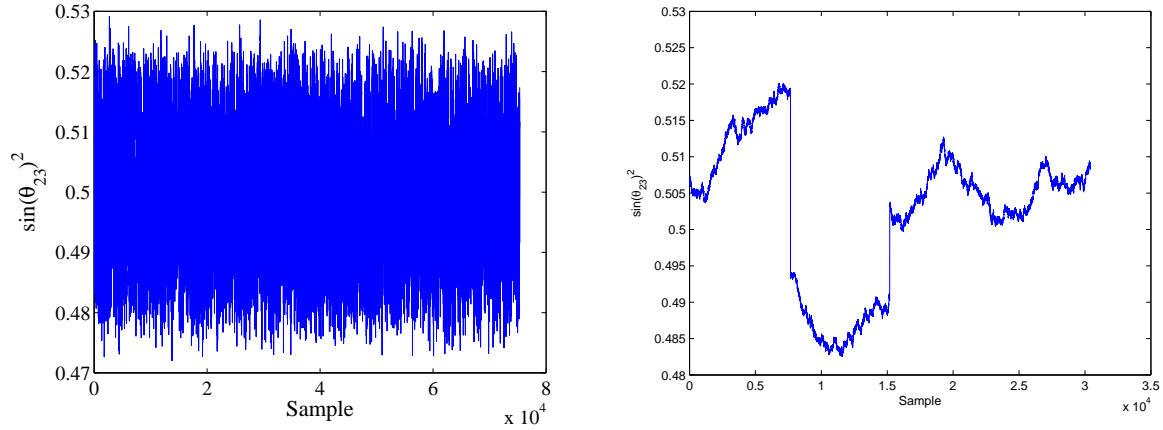
3.1.2 The C-library features

The C-library part of MonteCUBES provides all the methods necessary in order to perform MCMC simulations for neutrino oscillation experiments using the same experimental definition files as GLoBES. MonteCUBES uses a significant amount of the GLoBES functionality, which means that MonteCUBES can be used with any previously defined experimental definitions.

From a technical perspective, the basic features of MonteCUBES are very easy to use and provides a simple Metropolis sampling with a gaussian step proposal function $W(x \rightarrow y)$. It also provides several options for the checking of convergence and burn-in[3].

---

[2]Here, "less extreme" refers to a predefined ordering of the outcomes, such as double-sided intervals, upper/lower bounds, or Feldman-Cousins ordering [33].

[3]The "burn" of a MCMC is a number of samples in the beginning of the simulation that are thrown away.

Figure 5: Examples of one-dimensional chain progression plots for chains with good (left) as well as bad (right) convergence. See Ref. [31] for details.

3.1.3 The graphical interface

In addition to the C-library features, MonteCUBES is distributed along with a graphical user interface (GUI) for Matlab. The GUI provides methods for converting the C-library output into plots for diagnosis of the chains and for displaying the actual physical results. A perl script for users who do not have access to Matlab is under development.

Although MonteCUBES has the possibility to check convergence of the chains in run-time, it can be of interest to also check them manually using visual aids. For this purpose, the GUI provides two plotting options, the one-dimensional chain progression (see Fig. 5) and the two-dimensional parameter scatter (similar to Fig. 4). This type of plots can also be useful to tune the typical step size needed in the step proposal function $W(x \to y)$ in order to give fast convergence. Typically, the step size should be set to about the size of the region that is being explored by the chains.

The GUI also provides several possibilities for displaying the results of simulations. The basic type of plot is that of the most likely parts of the posterior probability distribution in one, two, or three dimensions. Apart from simply plotting the results against the parameters used in the simulation (such as θ_{23}), the GUI provides the possibility to plot the results against an arbitrary function of the parameters (such as $\sin^2(2\theta_{23})$). The GUI also includes the possibility of applying post-simulation priors through a weight function.

3.2 Advanced features

In addition to the basic functionality provided by MonteCUBES, it also contains several advanced features. First, the MCMC itself is highly customizable, allowing an advanced user to use essentially any step proposal function. As an intermediate step to this is the use of degeneracy steps, which provides the user with a powerful tool for exploring degenerate solutions in the same simulation (using only gaussian steps, this would require very long

---

This ensures that the actual chains will start closer to equilibrium, which will result in faster convergence.

11

simulations - especially if the degeneracies are well separated).

MonteCUBES is also distributed along with two additional features not related to the MCMC simulations. First, it includes the GLoBES implementation of two scenarios of new physics, NSI and non-unitarity. The second feature is the possibility to set the experimental event rates explicitly, which can be useful for analyzing actual data.

We have summarized the main features of MonteCUBES, a plugin for the simulation software GLoBES that provides the possibility to analyze neutrino oscillation experiments using MCMC methods. While doing so, we have discussed the advantages of using stochastic methods for exploring high-dimensional parameter spaces and why this is particlularly applicable to new physics in neutrino oscillations. Since MonteCUBES is a plugin for GLoBES, it can use any previously written experiment definition files and while the plugin itself is very simple to use, users already familiar with GLoBES will find it particularly easy to get started.

4 Review of Nufact Physics Potential

4.1 Sterile Neutrinos at a Nufact

In the last ten years, extensive work by many different collaborations has been devoted to the study of the potential of a Neutrino Factory facility to measure the parameters of the standard three-family PMNS mixing matrix that are still unknown (e.g., the mixing angle θ_{13}; the leptonic CP-violating phase δ; and the hierarchy between neutrino mass, i.e. the sign of the atmospheric mass difference). Since some consensus on the principal features of the Neutrino Factory design to be fullfilled to achieve these goals (see the Report of the *International Scoping Study for a Neutrino Factory and a Superbeam Facility*, [1], and the reports of the *International Design Study of a Neutrino Factory* for details), it is important to assess the potential of such a facility to study new physics beyond the standard three-family oscillations.

Within the possible straightforward extensions of the three-family oscillation model, we have studied in Ref. [4] the inclusion of one new light singlet fermion and the corresponding sensitivity of a Neutrino Factory facility to the four-family PMNS mixing matrix between three active neutrinos and the *sterile* one. The possible existence of a fourth light neutrino state was advanced to explain the LSND experiment data, which were consistent with $\nu_\mu \to \nu_e$ oscillations driven by a $\Delta m^2 \sim 1$ eV^2 mass difference, with an effective mixing angle $\sin^2 2\theta_{LSND} \sim 10^{-2}$ [34]. However, the MiniBooNE experiment (that was designed to check the LSND data) has found a negative result in the region of interest [35]. If we discard the possibility that O(1) eV singlet fermions could exist with an effective mixing angle $\theta_{LSND} \sim 3°$, it is still interesting to ask which is the ultimate sensitivity of existing, planned or future facilities to the parameter space of models with extra light singlet fermions.

Preliminar studies of four-neutrino models were performed at early stages of the Neutrino Factory optimization, [36–38], albeit using an ideal detector. A detailed study of the potential to study the four-neutrino model at the CNGS beam using the OPERA detector has been presented in Ref. [39].

4.1.1 The setups

Notice that this study can be performed either using the ISS/IDS design (optimized to look for three-family oscillation signals) or to look for modification of the baseline design that could improve the potential of the facility to new physics while keeping most of its potential to look for standard observables such as θ_{13} and δ, that would represent an unavoidable background to the search for deviations from the three-family PMNS model.

For this reason, we have compared two Neutrino Factory setups:

1. ISS/IDS-inspired Neutrino Factory

   It consists of a Neutrino Factory with 20 GeV muons stored into two storage rings aiming at two different baselines, with 50 Kton magnetized iron detectors of the MIND-type [40] located at $L = 4000$ Km and $L = 7500$ Km, respectively. The muons that decay in the straight section of the storage rings aiming at the detectors (useful muons) are 5×10^{20} per year per baseline (i.e., a total of 1×10^{21} useful muon decays per year).

2. High-energy Neutrino Factory

   In this case, we consider 50 GeV muons, again stored into two storage rings aiming at two different baselines, with 50 Kton magnetized iron detectors of the Hybrid-MIND-type [40] located at $L = 3000$ Km and $L = 7500$ Km, respectively. The Hybrid-MIND detector consists of a 4 Kton magnetized Emulsion Cloud Chamber (MECC) with iron plates intertwined with emulsion layers next to a 50 Kton MIND-type detector. The MECC section of the detector is needed to detect τ produced in $\nu_e \to \nu_\tau$ ("silver channel") and $\nu_\mu \to \nu_\tau$ ("discovery channel"). The muons that decay in the straight section of the storage rings aiming at the detectors (useful muons) are 2×10^{20} per year per baseline (i.e., a total of 4×10^{20} useful muon decays per year).

Realistic estimates of the efficiencies, of the backgrounds and of the systematic errors have been taken into account (see Ref. [4] for details).

4.1.2 Results

We have studied in Ref. [4] the extension of the standard three-family oscillation model with one extra singlet fermions, much heavier than the three active ones. This model is called the "3+1" model, and we parametrize the four-family mixing matrix as follows:
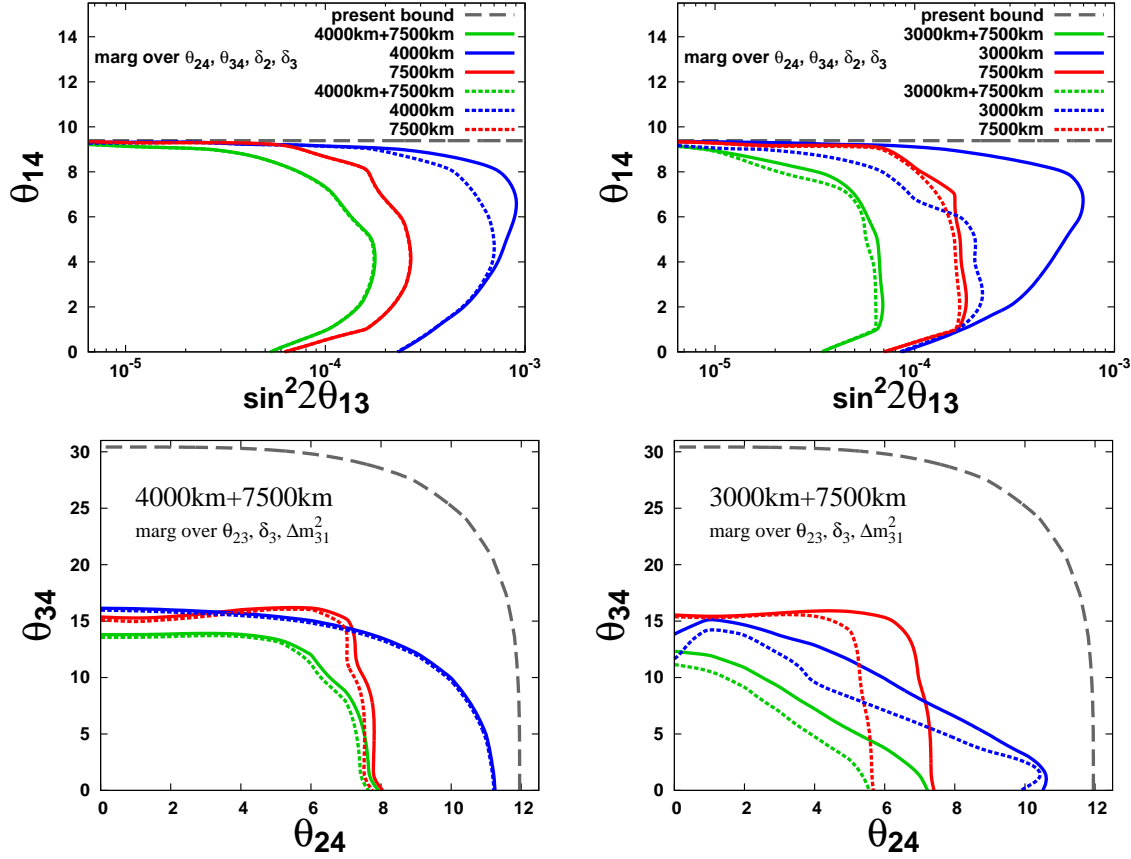
$$U_{PMNS} = U_{34}(\theta_{34})U_{24}(\theta_{24})U_{23}(\theta_{23}, \delta_3)U_{14}(\theta_{14})U_{13}(\theta_{13}, \delta_2)U_{12}(\theta_{12}, \delta_1) \quad (4)$$

The active-sterile mixing angles θ_{14} and θ_{24} are strongly bounded by electron disappearance experiments, and $s_{14} \sim s_{24} \sim s_{13}$. The angle θ_{34} can, on the other hand, reach values as large as $\theta_{34} \sim 30°$. It is therefore useful to expand in the following small parameters:

$$\epsilon \equiv \theta_{34} \sim \sqrt{\theta_{13}} \sim \sqrt{\theta_{14}} \sim \sqrt{\theta_{24}} \sim \sqrt{\delta\theta_{23}} \lesssim 4 \times 10^{-1},$$

with $\delta\theta_{23} = \theta_{23} - \pi/4$. At third order in ϵ, the oscillation probabilities in matter are:

$$P_{ee} \sim 1 + O\left(\epsilon^4\right) ; \quad P_{e\mu} \sim P_{e\tau} \sim P_{es} \sim O\left(\epsilon^4\right),$$
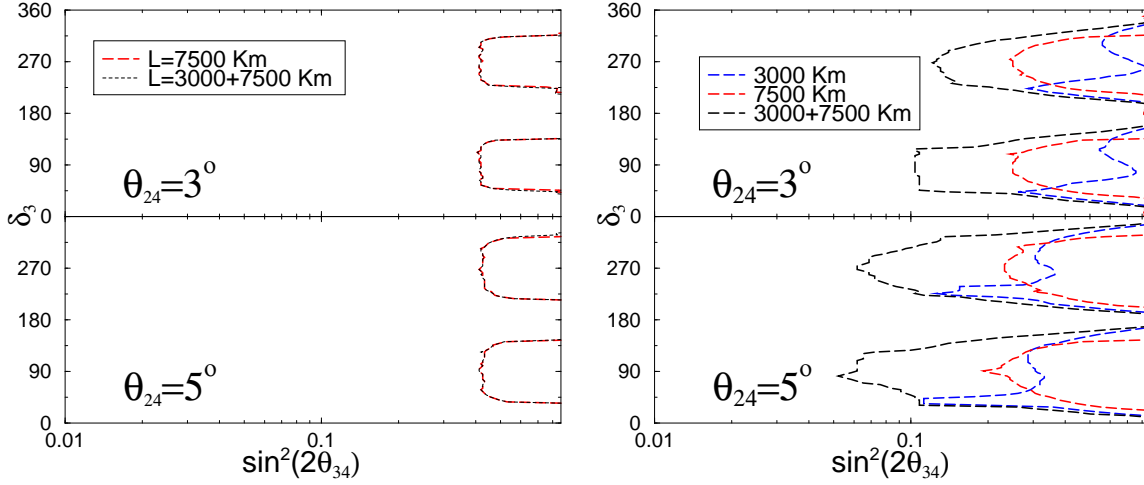
13

Figure 6: Sensitivity limit at 90% CL in the ($\sin^2 2\theta_{13}$, θ_{14}) plane (above) and in the (θ_{24}, θ_{34}) plane (below), marginalizing over the parameters not shown. The dashed grey line represent the present bounds on these parameters. The solid lines refer to MIND data ($\nu_e \to \nu_\mu, \nu_\mu \to \nu_\mu$), only. Dashed lines stand for Hybrid-MIND data (combination of the previous channels with $\nu_e \to \nu_\tau$ and $\nu_\mu \to \nu_\tau$ data). The colors are: blue for the shortest baseline; red for longest baseline; green for the combination of the two baselines. Left panels: 20 GeV NF; Right panel: 50 GeV NF. Taken from Ref. [4].

$$P_{\mu\mu} = 1 - \sin^2 \frac{\Delta_{31} L}{2} - 2 (A_n L) s_{24} s_{34} \cos \delta_3 \sin \Delta_{31} L + O\left(\epsilon^4\right) , \tag{5}$$

$$P_{\mu\tau} = \left(1 - s_{34}^2\right) \sin^2 \frac{\Delta_{31} L}{2} + \left\{ s_{24} s_{34} \sin \delta_3 + .2 (A_n L) s_{24} s_{34} \cos \delta_3 \right\} \sin \Delta_{31} L + O\left(\epsilon^4\right),$$

where $\Delta_{31} = \Delta m_{31}^2 / 2E$, and $|\Delta m_{31}^2|$ is Δm_{atm}^2, which is determined by the two-flavor analysis of the atmospheric neutrino data. The matter density parameter A_n is $A_n = \sqrt{2} G_F n_n / 2$, with n_n the number density of neutrons [41, 42]. We can see from these oscillation probabilities that $P_{\mu\tau}$ has an $O(\epsilon^2)$ sensitivity to sterile neutrinos through the s_{34}^2 terms, whereas both $P_{\mu\tau}$ and $P_{\mu\mu}$ have sensitivity to the non-standard CP-violating phase δ_3 through the $O(\epsilon^3)$ term in $s_{24} s_{34}$. The potential relevance of the $\nu_\mu \to \nu_\tau$ channel to search for non-standard physics motivates the high-energy Neutrino Factory setup, designed to improve the sensitivity to $\nu_e \to \nu_\tau$ and $\nu_\mu \to \nu_\tau$. Since the $\nu_\tau N$ CC cross-section is strongly suppressed with respect to the $\nu_e N, \nu_\mu N$ CC ones at low neutrino energies due to the τ mass, a beam

Figure 7: The 99% CL δ_3-discovery potential in the (θ_{34}, δ_3)-plane at the 50 GeV Neutrino Factory, for two values of θ_{24}, $\theta_{24} = 3°$ (above) and $5°$ (below). Left: $\nu_\mu \to \nu_\mu$ data, only; Right: combination of $\nu_\mu \to \nu_\mu$ and $\nu_\mu \to \nu_\tau$ data. Blue lines: 3000 Km data; red lines: 7500 Km data; black lines: combination of the two baselines. Taken from Ref. [4].

with high-energy neutrinos (with respect to the ISS/IDS setup) is desirable to increase the statistics in these channels.

In Fig. 6 we present the sensitivity at 90% CL to θ_{13} and to the active-sterile mixing angles θ_{14}, θ_{24} and θ_{34} in case of a null result. In the top panels, we can see that the 50 GeV Neutrino Factory setup (right) performs a bit better than the 20 GeV one (left), and that the inclusion of silver channel data ($\nu_e \to \nu_\mu$) plays a marginal role once two baselines are considered. In the bottom panels, on the other hand, we see that the 50 GeV facility performs much better than the 20 GeV one (when the two baselines are combined) and that the inclusion of $\nu_\mu \to \nu_\tau$ data has a non-negligible impact on the sensitivities.

In Fig. 7 we can see the δ_3-discovery potential of the 50 GeV Neutrino Factory in case of a positive result as a function of θ_{34} for $\theta_{24} = 3°, 5°$ (since the sensitivity of $P_{\mu\mu}, P_{\mu\tau}$ to δ_3 depends on the term proportional to $s_{24}s_{34}$, for $\theta_{24} = 0$ the sensitivity is lost). In this case, the inclusion of the $\nu_\mu \to \nu_\tau$ data is very important: the discovery potential goes from $\sin^2 \theta_{34} \sim 4 \times 10^{-1}$ when only $\nu_\mu \to \nu_\mu$ data are considered (left) to 6×10^{-2} when $\nu_\mu \to \nu_\mu$ and $\nu_\mu \to \nu_\tau$ data are combined (right).

Summarizing, the 50 GeV (20 GeV) setup can constrain $\theta_{34} \leq 12°(14°)$ and $\theta_{24} \leq 5.5°(8°)$ through the combination of $\nu_\mu \to \nu_\mu$ and $\nu_\mu \to \nu_\tau$ data; $\sin^2 2\theta_{13}^{(4\text{fam})} \leq 6 \times 10^{-5}(1.5 \times 10^{-4})$, with a slight dependence on θ_{14}, through the "golden channel". We can not improve the present constraint on θ_{14} (a near detector would be particularly useful for this purpose). Eventually, the combination of $\nu_\mu \to \nu_\mu$ and $\nu_\mu \to \nu_\tau$ data is an extremely powerful tool to look for CP-violation beyond the standard three-family one.

4.2 Non-standard Interactions in matter at a Nufact

It is anticipated that tiny oscillation signals will be explored with a neutrino factory experiment through its high statistics and precise information on the energy dependence. They

are not restricted only to the standard oscillation signals, and we have a chance to discover non-standard signals which are an evidence of physics beyond the standard model. A non-standard neutrino interaction (NSI) emerges in many classes of models at the high energy scale, and it can be described as an effective four-fermion interaction at the electroweak scale. Our concern in this section is to investigate the sensitivities to the effective NSI in the neutrino factory and to find out the optimal setup for the NSI search.

A neutrino oscillation experiment can be classified into three parts — beam production (source), propagation, and detection, and NSIs can enter in all three parts. Since the sensitivities to NSIs at the source and the detection processes strongly depend on the setup of near detectors, the specification of the near detector setup is currently discussed (near detectors in a neutrino factory was studied in Ref. [8]). Here, we focus on the NSIs in the propagation process, which are parametrized as the additional matter effect potential in the neutrino propagation Hamiltonian:

$$
H = \frac{1}{2E} \left[U \begin{pmatrix} 0 & & \\ & \Delta m_{21}^2 & \\ & & \Delta m_{31}^2 \end{pmatrix} U^\dagger + a_{\text{CC}} \begin{pmatrix} 1 + \epsilon_{ee}^m & \epsilon_{e\mu}^m & \epsilon_{e\tau}^m \\ (\epsilon_{e\mu}^m)^* & \epsilon_{\mu\mu}^m & \epsilon_{\mu\tau}^m \\ (\epsilon_{e\tau}^m)^* & (\epsilon_{\mu\tau}^m)^* & \epsilon_{\tau\tau}^m \end{pmatrix} \right], \tag{6}
$$

where a_{CC} is the standard matter effect potential which is defined as $a_{\text{CC}} = 2\sqrt{2}G_F n_e E$ with the electron number density n_e. The experimental bounds to $\epsilon_{\alpha\beta}^m$ have been recently re-discussed in Refs. [43, 44], and the constraint from the loop-induced charged lepton flavour violating processes are revised. In Ref. [43], the authors concluded that there were no model-independent bounds from the loop-induced processes, and the bound to $|\epsilon_{e\mu}^m|$ is considerably relaxed according to the revision. The bounds from the current experimental data are summarized in Ref. [44], which are

$$
|\epsilon_{ee}^m| < 3.8, \qquad |\epsilon_{\mu\mu}^m| < 6.4 \times 10^{-2}, \qquad |\epsilon_{\tau\tau}^m| < 21,
$$

$$
|\epsilon_{e\mu}^m| < 3.3 \times 10^{-1}, \qquad |\epsilon_{e\tau}^m| < 3.1, \qquad |\epsilon_{\mu\tau}^m| < 3.3 \times 10^{-1}, \tag{7}
$$

at the 90 % confidence level. When one assume some *naturalness conditions*, $|\epsilon_{e\mu}^m|$ is much more strongly constrained [43]. Neutrino oscillation experiments are expected to have a good sensitivity to the less constrained NSIs which are associated especially with the tau flavour.

4.2.1   The setup

The current baseline setup IDS-NF 1.0 [45] includes total three detectors — two Magnetized Iron Neutrino Detectors (MIND), and one Emulsion Cloud Chamber (ECC) for tau neutrino detection. With these detectors, we can observe the golden channel, the disappearance channel, and the silver channel, and the combination of the channels helps to solve the parameter degeneracies among NSIs as in the standard oscillation parameters. In Refs. [5, 46], it was shown that the combination of the golden and the disappearance channel with the MINDs placed at $L = 4000$ km and $L = 7500$ km solved the correlation between $\epsilon_{e\tau}^m$ and $\epsilon_{\tau\tau}^m$, which was the only NSI combination severely correlated in the golden channel. Thus, if two MINDs are included in the experiment, one can safely study a sensitivity to each NSI separately without an ECC.

4.2.2 Results

The impact of an ECC in the NSI search was discussed in Ref. [5], in which the sensitivity to $\epsilon_{e\tau}^m$ was investigated by scanning the baseline of an ECC and fixing the MINDs at $L = 4000$ km and $L = 7500$ km. The results showed that the ECC was relevant only in the case that the baseline is taken to be about 4000 km. The optimum muon energy was also studied. When two MINDs are fixed at $L = 4000$ km and $L = 7500$ km, the sensitivities to $\epsilon_{e\tau}^m$, $\epsilon_{\mu\tau}^m$ and $\epsilon_{\tau\tau}^m$ are getting higher proportional to the muon energy up to about 20 GeV, and they are saturated in the energy range of $E_\mu > 20$ GeV. If we include an ECC set at $L = 4000$ km, the sensitivity to $\epsilon_{e\tau}^m$ is improved proportionally to energy even in $E_\mu > 20$ GeV, thanks to a synergetic effect. However, the improvement is not impressive (less than a factor of two at $E_\mu = 100$ GeV), because of the small statistics of the silver channel events. From the simulation studies, we can conclude that the ECC is not a key component to search for NSIs in the neutrino propagation process, when we already have two MINDs with the correct baseline configuration. Since a certain high energy (and also a long baseline) is an important ingredient to search for the NSI in propagation, the low energy alternative [47,48] of a neutrino factory, which has been recently developed, is not preferred for this purpose.

The baseline of MINDs was also optimized for the NSI search in Ref. [5], which showed that the optimal setup for the standard oscillation parameters, that is $L = 4000$ km and $L = 7500$ km, is also favourable for the $\epsilon_{e\tau}^m$ search. For the $\epsilon_{\mu\tau}^m$ and $\epsilon_{\tau\tau}^m$ search, an even longer baseline (such as a core-crossing baseline) is preferable. However, the advantage of taking a longer baseline is just about a factor of two.

The robustness of the optimization for the standard oscillation parameters with respect to the contamination of NSIs is also an important issue. When the additional fit of the NSI parameters is carried out, the sensitivities to the standard oscillation parameters are degraded somewhat. However, the optimal setup is hardly changed from $L = 4000$ km and $L = 7500$ km [5].

In the neutrino factory with two MINDs set at $L = 4000$ km and $L = 7500$ km and with $E_\mu = 25$ GeV (based on IDS-NF 1.0), the sensitivities to the propagation NSI $\epsilon_{\alpha\beta}^m$ at the 90 % confidence level are listed as follows [5]:

$$|\epsilon_{ee}^m| < 1.4 \times 10^{-1}, \qquad |\epsilon_{\mu\mu}^m| < 1.9 \times 10^{-2}, \qquad |\epsilon_{\tau\tau}^m| < 1.9 \times 10^{-2},$$

$$|\epsilon_{e\mu}^m| < 3.4 \times 10^{-3}, \qquad |\epsilon_{e\tau}^m| < 4.7 \times 10^{-3}, \qquad |\epsilon_{\mu\tau}^m| < 1.8 \times 10^{-2}. \tag{8}$$

From the comparison with Eq. (7), we can expect that the neutrino factory will improve the current bounds by one to three orders of magnitude. The epsilon parameters of the order of 10^{-2} to 10^{-3} naively correspond to physics at the TeV scale [49–52].

4.3 Non-unitarity mixing at a Nufact

Non-unitarity of the leptonic mixing matrix is a generic manifestation of new physics in the lepton sector. The MUV scheme [53] provides an effective field theory extension of the SM and is minimal in the sense that only three light neutrinos are considered and that new physics is only introduced in the neutrino sector, describing the relevant effects on neutrino oscillations in the various types of models where the SM is extended by heavy singlet fermions [54].

In this scheme, the charged and neutral-current interactions of the neutrinos are modified. The non-unitary leptonic mixing matrix N, which appears in the charged-current, interaction, contains the only additional degrees of freedom. Thus, instead of the three mixing angles and three CP-phases of the unitary PMNS leptonic mixing matrix (with only one affecting neutrino oscillations), the non-unitary mixing matrix N contains 15 parameters, out of which six are CP-violating phases (including two Majorana phases, which do not affect neutrino oscillations). The goal of this work is to study the potential of a Neutrino Factory [55, 56] in constraining or determining the whole parameter space of the MUV scheme, focusing in the new CP-phases associated.

4.3.1 The setup

Our set-up is the Neutrino Factory proposed in the International Design Study (IDS) [1, 45], which consists of ν_e and ν_μ beams from 5×10^{20} muon decays per year per baseline. We consider a setting where the experiment is assumed to run for five years in each polarity. The parent muons are assumed to have an energy of 25 GeV. The beams are detected at two far sites, the first located at 4000 km with a 50 kton Magnetised Iron Neutrino Detector (MIND) [40] and a 10 kton Emulsion Cloud Chamber (ECC) for τ detection [57, 58], and the second located close to the magic baseline [59, 60] at 7500 km with an iron detector identical to the one at 4000 km. In the simulations, we study the "golden" [61] $\nu_e \to \nu_\mu$ and ν_μ disappearance channels in the MIND detectors and the "silver" [57,58] $\nu_e \to \nu_\tau$ and "discovery" [4] $\nu_\mu \to \nu_\tau$ channels at the ECC detectors, both near and far. The detector efficiencies and backgrounds considered are described in [6]. We scan the complete MUV parameter space, adding nine unitarity-violating parameters to the six standard neutrino oscillation parameters. The scan is performed using the MonteCUBES software [3, 31].

4.3.2 Results

First of all, let us parametrize the mixing matrix N taking advantage from the fact that a general matrix can be written as the product of a Hermitian matrix times a unitary matrix. Writing the Hermitian matrix as $\mathbb{1} + \varepsilon$ (with $\varepsilon = \varepsilon^\dagger$) and denoting the unitary matrix by U, we can write [62]
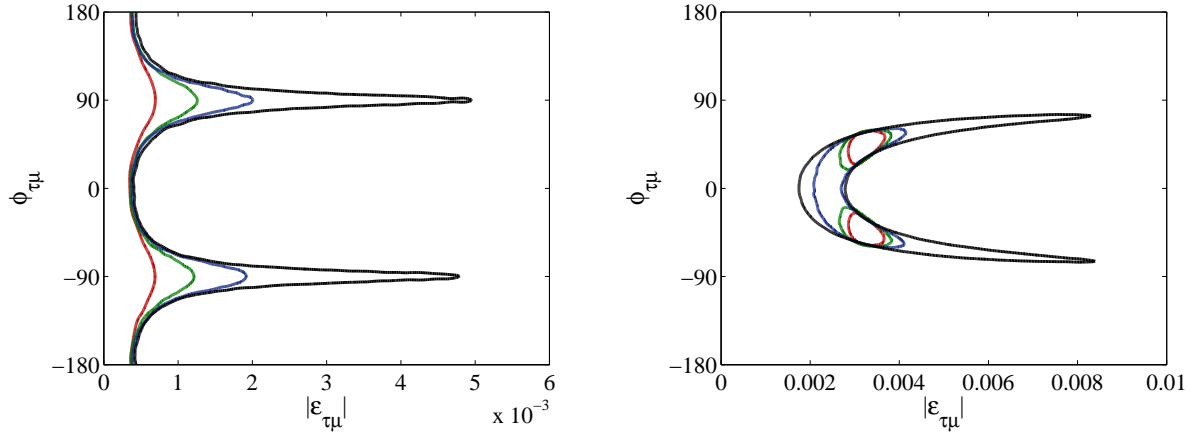
$$N = (\mathbb{1} + \varepsilon) U . \tag{9}$$

where $\varepsilon_{\alpha\beta} = |\varepsilon_{\alpha\beta}| e^{i\phi_{\alpha\beta}}$ for $\alpha \neq \beta$. The present 90 % CL bounds[4] are $|\varepsilon_{\mu e}| < 3.5 \times 10^{-5}$, $|\varepsilon_{\tau e}| < 8.0 \times 10^{-3}$, $|\varepsilon_{\tau\mu}| < 5.1 \times 10^{-3}$ [53] and $|\varepsilon_{ee}| < 2.0 \times 10^{-3}$, $|\varepsilon_{\mu\mu}| < 8.0 \times 10^{-4}$, $|\varepsilon_{\tau\tau}| < 2.7 \times 10^{-3}$ [51].

Before to present the more relevant results of our simulations, we would like just to stress the importance of studying the "zero-distance effect" with near detectors. If the flavour basis is not orthogonal, it translates to a baseline-independent term in the oscillation probabilities:

$$P_{\alpha\beta}(L = 0) = 4|\varepsilon_{\alpha\beta}|^2 + \mathcal{O}(\varepsilon^3), \quad \alpha \neq \beta \tag{10}$$

---

[4]Violation of unitarity can arise both in the production and in the detection processes. Coefficients parametrizing the former are usually labelled $\epsilon^s_{\alpha\beta}$, the latter as $\epsilon^d_{\alpha\beta}$. In the MUV scheme, $\epsilon^s = \epsilon^d = \epsilon$.

Figure 8: The 90 % confidence level sensitivity of the IDS Neutrino Factory to the unitarity-violating parameters $\varepsilon_{\tau\mu}$ (left), and sensitivity assuming that it takes the value $\varepsilon_{\tau\mu} = 3.2 \times 10^{-3} \exp(i\pi/4)$ (right). The different curves correspond to different sizes of the near τ detector, from left to right, 10 kton, 1 kton, 100 ton, no near detector. Taken from Ref. [5].

This term is best probed at short distances, since the flux is larger and it cannot be hidden by the standard oscillations. Near detectors are, thus, excellent for probing the zero-distance effect, in particular τ detectors are of importance, since the present bounds on $\varepsilon_{\mu e}$ and $\varepsilon_{\mu\mu}$ are rather strong. We will therefore study the impact of near τ detectors of different sizes located at 1 km from the beam source. In particular, we will present all the results for near detector sizes of 100 ton, 1 kton, and 10 kton, as well as the results without any near τ detector.

One of the most remarkable features resulting from our simulations is that the results do not contain significant correlations between any of the unitarity-violating parameters, nor are the unitarity-violating parameters significantly correlated with the standard neutrino oscillation parameters. The only exception are some mild correlations between θ_{13}, δ and the modulus and phase of $\varepsilon_{\tau e}$ in the absence of near τ detectors which, however, do not lead to new degeneracies between these parameters or spoil the determination of θ_{13} and δ at the Neutrino Factory. Furthermore, the addition of a near τ detector of only 100 ton is enough to almost completely erase these correlations. This implies that the Neutrino Factory setup considered here has enough sensitivity to distinguish the effects induced by unitarity-violation from changes in the standard parameters. Second, the sensitivities of the Neutrino Factory to the diagonal parameters of the ε matrix, as well as to $\varepsilon_{\mu e}$, do not improve with respect to the bounds derived from electroweak decays, which are too stringent to allow for observable effects at the Neutrino Factory. In addition, we find that a near τ detector with a mass as small as 100 ton would dominate the sensitivity to $\varepsilon_{\tau e}$ through the measurement of the zero-distance effect, providing sensitivities down to $\mathcal{O}(10^{-3})$.

Now, we will thus concentrate on the sensitivities to $\varepsilon_{\tau\mu}$, even though the other unitarity-violating parameters and standard oscillation parameters are allowed to vary in the simulations. In the left panel of Fig. 8, we show the sensitivity to the $\varepsilon_{\tau\mu}$ parameter for the four different sizes considered for the near ECC. The input values for all the non-unitarity

parameters and θ_{13} were set to zero to derive these curves. We have checked that the results do not depend strongly on this assumption. The most remarkable feature of this figure is the extreme sensitivity to the real part of $\varepsilon_{\tau\mu}$ which is present already without any near detector. This sensitivity mainly originates from the matter effect on the disappearance channel, where the leading non-unitarity correction to the oscillation probability is given by

$$\hat{P}_{\mu\mu} = P_{\mu\mu}^{\mathrm{SM}} - 2\,\mathrm{Re}(\varepsilon_{\mu\tau})AL\sin\left(\frac{\Delta m_{31}^2 L}{2E}\right) + ...\,, \tag{11}$$

where $A = \sqrt{2}G_F n_e$. The terms we have omitted in the above equation, as well as expanded expressions for the rest of the probabilities, can be found in Ref. [6]. Notice that the $\nu_\mu \to \nu_\tau$ channel also depends linearly on $\varepsilon_{\tau\mu}$ (see [6]) and that the dependence is CP-violating. On the other hand, the mass and efficiency of the ECC detector are much smaller compared to those of the MIND detectors for the ν_μ disappearance channel and therefore the sensitivity is dominated by the latter. As can be seen in the figure, a near τ detector will determine the modulus of $\varepsilon_{\mu\tau}$ through the zero-distance effect. This would translate into a vertical band in the left panel of Fig. 8 and thus the increase of the mass of the near detector improves the measurement of the imaginary part. However, given the linear dependence due to the matter effects on propagation, the bound on the real part from the disappearance channel remains stronger. We can also see that the bound on the modulus does not require a very large near detector, the bound on the imaginary part is essentially only improved by approximately 30 % in moving from a 1 kton to a 10 kton ECC detector.

Another important question is how well the Neutrino Factory would be able to measure the unitarity-violating parameters if they are non-zero. For this reason, in the right panel of Fig. 8, we show the sensitivity to $\varepsilon_{\tau\mu}$ assuming that $|\varepsilon_{\tau\mu}| = 3.2 \times 10^{-3}$ as well as $\phi_{\tau\mu} = 45°$ which is disfavoured at only 1σ by current bounds. Again, we can see that the sensitivity without the near detector is only to the real part of $\varepsilon_{\tau\mu}$. In this setting, there is a degeneracy extending essentially as $|\varepsilon_{\tau\mu}| \propto 1/\cos(\phi_{\tau\mu})$, along which the real part of $\varepsilon_{\tau\mu}$ is constant and the imaginary part is changing. The introduction of near detectors results in an effective measurement of $|\varepsilon_{\tau\mu}|$, $i.e.$, a vertical band in the plot, which intersects the far detector measurement giving rise to two degenerate solutions, one for positive and one for negative phase value. Again, the actual size of the near detector is not crucial and no significant gain is seen beyond 1 kton.

These figures also show the strong complementarity between the near and far detectors when it comes to measuring the phase of the unitarity-violating parameter, and thus also a non-standard source of CP-violation. Neither the near nor the far detectors alone can establish a CP-violating phase by themselves. However, combining the two results excludes CP-conservation at 90 % confidence level.

Taking into account the results just presented above, we conclude that a Neutrino Factory would provide powerful tool for probing unitarity-violation in the leptonic mixing matrix. For the parameters to which it is most sensitive, the sensitivity is an order of magnitude better than the current experimental bounds. On the other hand, the interplay between the near and far detectors would allow to test new sources of CP-violation in the lepton sector.

4.4 Critical assessment on long baseline tau neutrino detection at Nufact

4.4.1 Standard oscillation physics

The prime focus of a neutrino factory is to provide precision measurements or tight constraints on the three-flavor oscillation parameters. Many studies done in the context of the ISS [1,63] show that the potential to achieve this is excellent if it is ensured that parameter correlations and degeneracies can be resolved. Any single rate measurement at some fixed baseline L and neutrino energy E is sensitive only to a *combination* of parameters. To measure all parameters separately, the following possibilities exist to resolve the correlations and degeneracies:

- **Use measurements at different energies.** This is difficult at a neutrino factory due to the limited width of the neutrino spectrum and the limited energy resolution of the MIND detector. It has been shown that the energy resolution of MIND is not enough for a single detector located at intermediate baseline to solve all of the degeneracies.

- **Perform measurements at two different baselines L_1 and L_2.** This is an extremely powerful possibility, which is the reason, it is included in the current IDS-NF baseline setup. In particular, a measurement at the magic baseline [60] turns out to be very important. A detailed optimization study for L_1 and L_2 has been performed in [5], with the result that the combination $L_1 = 4\,000$ km, $L_2 = 7\,500$ km is optimal to study standard oscillation physics as well as non-standard neutrino interactions.

- **Study different oscillation channels.** With MIND detectors, the Golden ($\nu_e \to \nu_\mu$) and Disappearance ($\nu_\mu \to \nu_\mu$) channels are available, while an inclusion of a ν_τ detector could in addition provide a window on the Silver ($\nu_e \to \nu_\tau$) and Discovery ($\nu_\mu \to \nu_\tau$) channels. Ref. [5], however, shows that the combination of one MIND detector and one ECC at the intermediate baseline is not as good as the combination of two MINDs at two baselines, mainly because of the very low statistics at the τ-detector for $\theta_{13} \leq 2°$. On the other hand, adding one ECC to the setup with two MINDs does not provide more than a marginal gain in sensitivity, independently of the neutrino energy and baseline. The reason is that the analytical expressions for the oscillation probabilities in the Golden and Silver channels are very similar (they differ only in the signs of certain terms and in the exchange $\sin\theta_{23} \leftrightarrow \cos\theta_{23}$ in several others), so that the Silver channel could help only to resolve degeneracies. This, however, is already done by the combination of the two Golden channel detectors. We, also, have checked numerically that also the inclusion of the Discovery channel does not improve the sensitivity of the neutrino factory to standard three-flavor oscillations.

  In Ref. [64], the silver channel was studied to solve the octant degeneracy and as a tool to study deviations from maximality of the atmospheric angle θ_{23}. A comprehensive study of alternatives to the silver channel for these tasks is lacking, see Ref. [65]. A likely outcome of such a study will be that alternatives are better than the silver channel. However, in the absence of such a study, we cannot draw a firm conclusion.

As for the standard three-family oscillations, we thus believe that an ECC detector able to look for $\nu_e \to \nu_\tau$ and $\nu_\mu \to \nu_\tau$ channels will not improve significantly the performances of the baseline neutrino factory setup with two MINDs , due to the strong statistical limitations of the present detector design and to the relatively limited number of parameters to be measured.

4.4.2   Non-standard oscillation physics

There are several interesting cases of new physics that can be studied through neutrino oscillation experiments. We will address here the potential of a detector capable of τ-identification in searching for Non-Standard Interactions (NSI) or additional singlet fermions with some admixture with the three-family left-handed neutrinos, so-called "sterile neutrinos".

Non-standard interactions are effective four-fermion interactions, which arise if neutrinos couple to new, heavy particles. This is similar to the Fermi theory of nuclear beta decay emerging as the low-energy fingerprint of the Standard Model weak interactions. NSI can affect the neutrino production and detection mechanism if they are of the charged current type, and the neutrino propagation if they are of the neutral current type. In the first case, the NSI can be parametrized as a small admixture of the "wrong flavor" $|\nu_\beta\rangle$ to a neutrino produced or detected in association with a charged lepton of flavor α:

$$|\nu_\alpha^s\rangle = |\nu_\alpha\rangle + \sum_{\beta=e,\mu,\tau} \varepsilon_{\alpha\beta}^s |\nu_\beta\rangle, \qquad\qquad \text{e.g. } \pi^+ \xrightarrow{\varepsilon_{\mu e}^s} \mu^+ \nu_e \qquad (12)$$

$$\langle\nu_\alpha^d| = \langle\nu_\alpha| + \sum_{\beta=e,\mu,\tau} \varepsilon_{\beta\alpha}^d \langle\nu_\beta| \qquad\qquad \text{e.g. } \nu_\tau N \xrightarrow{\varepsilon_{\tau e}^d} e^- X . \qquad (13)$$

The second case corresponds to a non-standard contribution to the MSW potential:

$$\tilde{V}_{\text{MSW}} = \sqrt{2} G_F N_e \begin{pmatrix} 1+\varepsilon_{ee}^m & \varepsilon_{e\mu}^m & \varepsilon_{e\tau}^m \\ \varepsilon_{e\mu}^{m*} & \varepsilon_{\mu\mu}^m & \varepsilon_{\mu\tau}^m \\ \varepsilon_{e\tau}^{m*} & \varepsilon_{\mu\tau}^{m*} & \varepsilon_{\tau\tau}^m \end{pmatrix} . \qquad (14)$$

In the above expressions, the parameters $\varepsilon_{\alpha\beta}^{s,d,m}$ give the strength of the NSI relative to standard weak interactions. A generic estimate is

$$|\varepsilon_{\alpha\beta}^{s,d,m}| \sim \frac{M_{\text{W}}^2}{M_{\text{NSI}}^2}, \qquad (15)$$

where M_{NSI} is the new physics scale, at which the effective NSI operators are generated. Even though the present model independent bounds on the $\varepsilon_{\alpha\beta}^{s,d,m}$ are not very strong ($\mathcal{O}(0.1-1)$). However, these bounds are not likely to be saturated in specific models [51, 52]; at least if one follows the usual guidelines of model building: no fine-tuning, as few new particles as possible, new physics preferably at or above the TeV scale, *etc.* Indeed, if the estimate (15) is taken at face values, with $M_{\text{NSI}} \sim 1$ TeV, we expect $\varepsilon_{\alpha\beta}^{s,d,m} < 0.01$. It is important to keep in mind that, in any specific model, the phenomenological parameters $\varepsilon_{\alpha\beta}^{s,d,m}$ will in general not be independent.

Phenomenological models in which N new singlet fermions are mixed with the three left-handed ones imply a straightforward generalization of the PMNS matrix to a $(3+N)\times(3+N)$ unitary mixing matrix, that for the case of $N = 1$ is:

$$U_{\text{PMNS}} = \begin{pmatrix} U_{e1} & U_{e2} & U_{e3} & U_{e4} \\ U_{\mu 1} & U_{\mu 2} & U_{\mu 3} & U_{\mu 4} \\ U_{\tau 1} & U_{\tau 2} & U_{\tau 3} & U_{\tau 4} \\ U_{s1} & U_{s2} & U_{s3} & U_{s4} \end{pmatrix} \tag{16}$$

Some of these elements are strongly constrained by non-observation at reactors and at the MiniBooNE experiment. On the other hand, models in which the mixing angles θ_{i4} between a new singlet fermion ν_s and the three active ones are all very small cannot be excluded. Notice that, both for NSI and sterile neutrino models, new CP-violating phases are present in addition to the standard three-family oscillation phase δ.

1. **NSI in production and detection**

   NSI in production and detection imply non-unitarity of the PMNS matrix. Therefore, if some of the new parameters $\epsilon_{\alpha\beta}^{s,d}$ are non-vanishing, it is not enough to study the two channels available at the MIND detector (the $\nu_e \to \nu_\mu$ golden channel and the $\nu_\mu \to \nu_\mu$ disappearance channel) to measure all of the new parameters of the model. To study non-unitarity of the leptonic mixing matrix, there are two options:

   - Measure all the oscillation probabilities $P(\nu_\mu \to \nu_e)$, $P(\nu_\mu \to \nu_\mu)$, $P(\nu_\mu \to \nu_\tau)$ (or $P(\nu_e \to \nu_e)$, $P(\nu_e \to \nu_\mu)$, $P(\nu_e \to \nu_\tau)$, and check if they sum up to unity. A problem of this approach is that ν_e detection is very difficult in a MIND detector, so either there will be large uncertainties or a secondary detector with a different technology (for example, liquid argon) should be added to the two MINDs setup. Moreover, the systematical errors in the different oscillation channels will be different, which also limits the achievable sensitivity.

   - Use neutral current events. This is also difficult [66], and, at present, only a sensitivity at the ten per cent level can be achieved. This might improve if the neutral current cross sections were known better and if more sophisticated event selection criteria could be developed.

   Most of the new parameters could be measured using a dedicated near detector. The detector design should be optimized so as to measure as much oscillation channels as possible, and with very good τ-identification capability. Therefore, this detector cannot be a scaled version of MIND. At present, no detailed study of such a detector has been performed, see Refs. [51, 52] for the potential of an ECC near to a Neutrino Factory source and the recent Ref. [8].

2. **NSI in propagation**

   NSI in propagation do not imply a non-unitary PMNS matrix. In this case it is therefore possible to obtain information on all of the new parameters $\epsilon_{\alpha\beta}^m$ using the two channels available at the MIND detector.

A detailed study of NSI in propagation at a neutrino factory has been presented in Ref. [5] (see fig. 9, taken from that paper). The results obtained show that the IDS-NFS baseline neutrino factory with two MIND detectors at $L \sim 4000$ km and $L \sim 7500$ km is sensitive to $\varepsilon_{\alpha\beta}^m \sim 0.01 - 0.1$, independent of whether a ν_τ detector is present. There might be a physics case for this detector if the process $\nu_\tau + N \to \tau + X$ proceeds in an unexpected way (e.g. an anomalous energy dependence), if τ leptons are produced in a non-standard way (e.g. $\varepsilon_{e\tau}^d \neq 0$ or $\varepsilon_{\mu\tau}^d \neq 0$), or if the muons stored in a neutrino factory have a small branching to ν_τ, e.g. due to $\varepsilon_{\mu\tau}^s \neq 0$ or $\varepsilon_{e\tau}^s \neq 0$. In the first case, a ν_τ detector at around the first oscillation maximum would be required because the ν_τ flux first has to be generated by oscillation from ν_μ; in the second case, a ν_τ *near* detector would be optimal due to the higher flux at the near site.

From this analysis, we conclude that an ECC detector to look for τ's produced through $\nu_e \to \nu_\tau$ does not improve the expected IDS-NF baseline setup sensitivity to NSI in propagation. A thorough study of the impact of $\nu_\mu \to \nu_\tau$ data is lacking, though. We do not expect, however, these data to have a striking impact on the sensitivity, due to unitarity of the PMNS matrix in models in which only NSI in matter are considered.
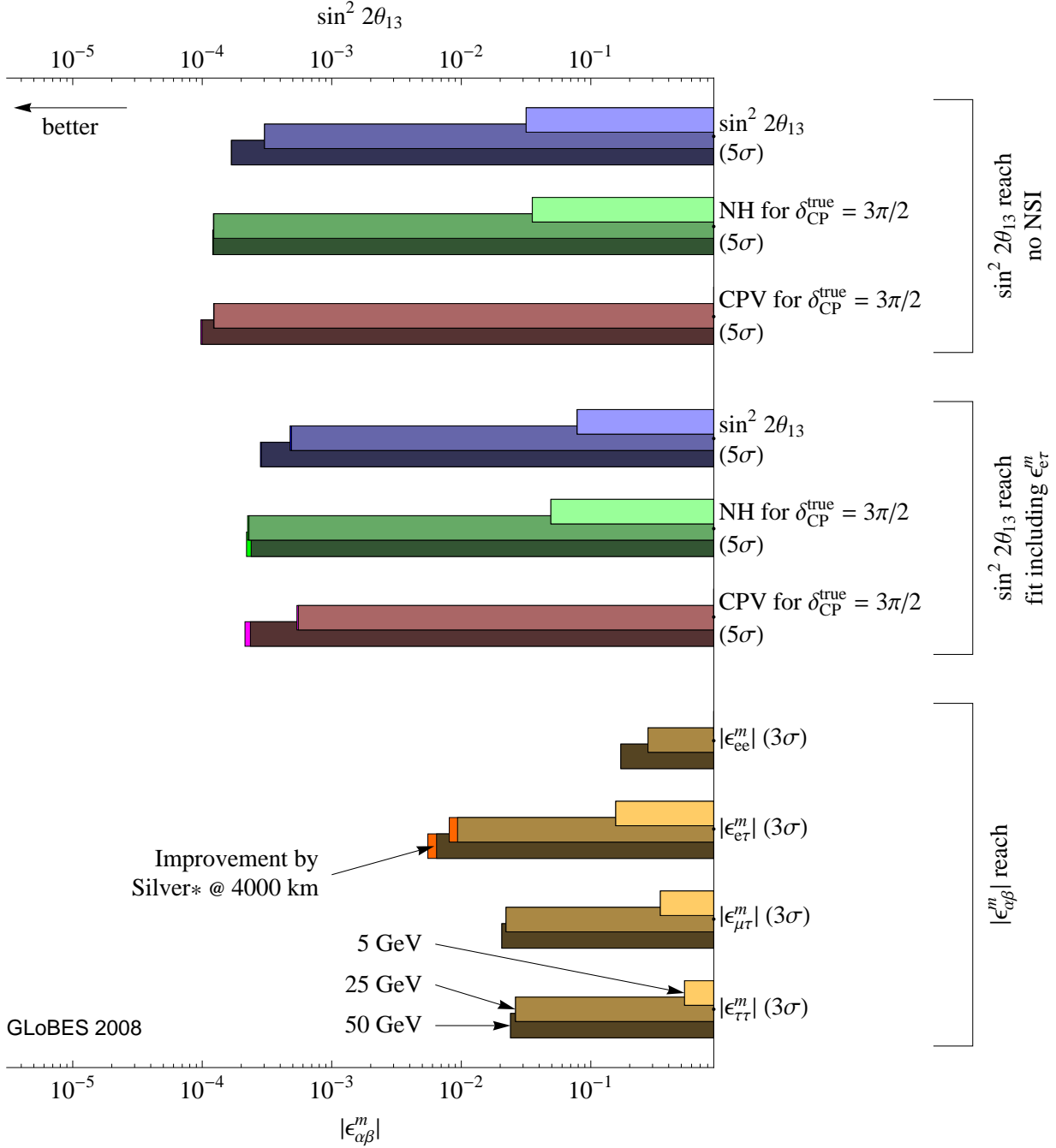
3. **Sterile neutrinos**

Even though sterile neutrinos do no longer receive as much attention nowadays as before the publication of the MiniBooNE results, they are still a viable possibility, motivated by the fact that neutral singlets ν_s appear in many models of new physics. If they are light, the neutrinos produced in a neutrino factory may have a small admixture of ν_s, while heavy ν_s (such as right-handed Majorana neutrinos in type-I see-saw models) would manifest themselves in the form of a non-unitary mixing matrix of the light neutrinos.

In the case of one light ν_s, a recent study [4] shows that the $\nu_\mu \to \nu_\tau$ appearance channel (mostly disregarded up to now; see, however, Ref. [67]), measured with a magnetized ECC, is extremely important when combined to $\nu_\mu \to \nu_\mu$ to measure some of the parameters of the model, and in particular some of the new CP-violating phases. On the other hand, the silver channel $\nu_e \to \nu_\tau$ is only of limited impact when added to the golden channel $\nu_e \to \nu_\mu$, although it is useful to solve some of the many degeneracies in the parameter space.

A criticism to the use of magnetized ECC to study the $\nu_\mu \to \nu_\tau$ channel is that the scanning load could be too high for this analysis to be realistic. However, it has been found that the scanning load for an emulsion detector at $L > 1\,000$ km is not huge: $O(500)$ events per kton per year with a 2×10^{20} flux are expected , for perfect efficiency. Adding a similar number of background events, this scanning load is compatible with extrapolation for present capabilities

Notice that for standard three-family oscillation and in models with NSI in propagation, due to the unitarity of the PMNS matrix, a good knowledge of the golden and the disappearance channel (both studied at MIND) should be enough to explore the whole parameter space. This, however, is not the case in models in which the 3×3 PMNS matrix is not unitary. In sterile neutrino models, for example, since we are not able to study the $\nu_\mu \to \nu_s$ appearance channel(s), the information that can

Figure 9: Summary of the neutrino factory performance with and without the presence of non-standard interactions. The IDS-NF setup with two MIND detectors at $L_1 = 4\,000$ km, $L_2 = 7\,500$ km was used, and the "true" parameter values $\sin^2 2\theta_{13} = 0.001$ and $\delta_{CP} = 3\pi/2$ were assumed. The plot shows that sensitivities are poor at $E_\mu = 5$ GeV (light bars), but increase dramatically at $E_\mu = 25$ GeV (medium light bars). The benefit from increasing E_μ further to 50 GeV (dark bars) is only marginal, as is the benefit from including a silver channel detector. Figure taken from [5]; see that paper for details.

be extracted from the ν_μ disappearance channel and the $\nu_\mu \to \nu_\tau$ channel are not identical. The same would happen in extensions of the standard model in which NSI are considered both in propagation and production, such as to violate unitarity of the PMNS matrix.

From the analysis of Ref. [4] we conclude that the combination of the IDS-NF baseline setup (with two MINDs) with one or two magnetized ECC increase significantly the potential of the Neutrino Factory to measure all the parameter space of the (3+1)-neutrino model and, in particular, to increase its CP-violation discovery potential. However, it has been shown that the present design of the magnetized ECC is not optimized and that a dedicated study of the detector to look for new physics is mandatory (see next section).
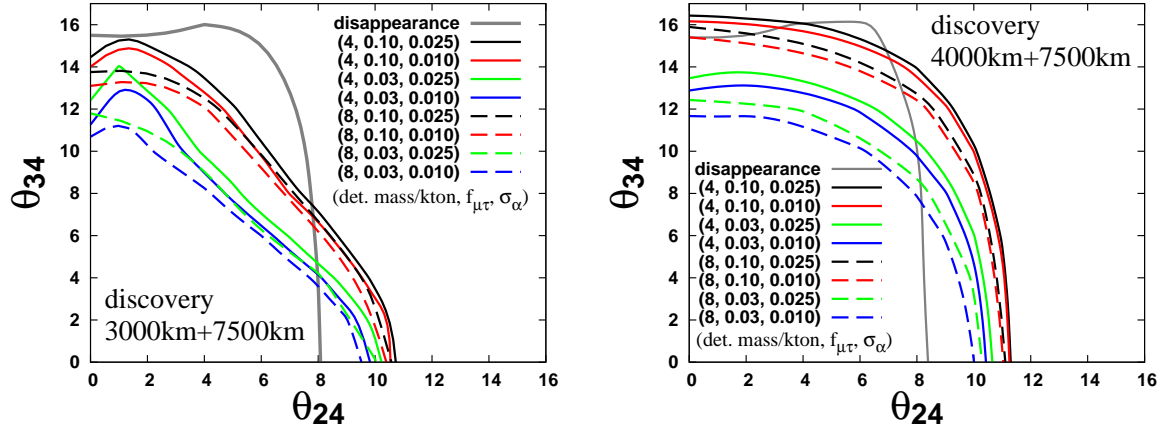
The optimal location for a long baseline τ-detector to study sterile neutrinos is not clear, yet. Whereas a detector whose purpose is the study of the silver channel in the framework of the three-family model or NSI in propagation is optimally located around the intermediate IDS-NF baseline (see ISS Final Report and Ref. [5]), it seems that to study (3+1) sterile neutrinos to put the magnetized ECC detector at the Magic Baseline could be more convenient. This is particularly true for searches of CP-violating signals. At the Magic Baseline, indeed, the standard three-family CP-violating effect vanishes, and therefore if CP-violation is observed this is clearly pointing out the existence of physics beyond the standard model (either new particles, such as the sterile neutrinos, or new effective operators, such as in NSI). Notice that the $\nu_\mu \to \nu_\tau$ statistics at the Magic Baseline is still large (of O(500) events for 1 kton MECC with perfect efficiency and 2×10^{20} useful muons per year).

4.4.3 Technological options for τ-detectors

The technology for tau-detectors has not been fixed yet. The liquid argon technology should be studied further (something compatible with the time scale of a Neutrino Factory). Furthermore, the impact of systematics errors in the magnetized emulsion technique (MECC) is shown to be very important, see Fig. 10.

In the figure, the sensitivity to two parameters of a model with three active and one sterile neutrino (the "3+1" model) using the $\nu_\mu \to \nu_\tau$ channel is shown. The dashed gray line refers to the sensitivity to those parameters achievable using two 50 kton MIND detectors: one at an intermediate baseline, $L = 3000 - 4000$ km, and the second at the Magic Baseline. In the two panels, we show the sensitivity for a 50 GeV muon Neutrino Factory (left) and a 20 GeV muon Neutrino Factory (right). It is clear from the left panel that a huge increase in the sensitivity of the $\nu_\mu \to \nu_\tau$ channel is achieved if the uncorrelated systematic errors are reduced from 10%(black solid line) to 3% (green solid line). This improvement is actually much more important than an increase in the MECC detector mass from 4 kton (green solid line) to 8 kton (green dashed line).

This systematic error is taking into account in a non-detailed way systematics induced by normalization of the flux and cross-sections. Both are expected to be better known after the first OPERA phase. Moreover, $\nu_\tau N$ cross-sections must be studied with a near detector, as it happens for the $\nu_\mu N$ one. This means that these sources of systematics can be strongly

Figure 10: Left (right) panel: Dependence of the excluded region in the $(\theta_{24}, \theta_{34})$-plane on the systematic errors $f_{\mu\tau} \equiv f_j$ and σ_α for the discovery channel $(\nu_\mu \to \nu_\tau)$ as well as the MECC detector mass at the 50 GeV (20 GeV) neutrino factory, where the excluded regions are by the discovery channel only. The solid (dashed) lines assume 4 kton (8 kton) for the tau detector mass. The solid gray line, which stands for the excluded region by the ν_μ disappearance channel, is also shown. Taken from Ref. [4].

reduced. A study of the possible improvement of the sensitivity with a better design of the τ-detector in the framework of NSI extensions of the standard model is lacking.

4.4.4 Conclusions & recommendations

In this note, we have discussed the potential of an ECC, added to the IDS-NF baseline setup (with two MIND detectors located at $L \sim 4000$ km and at the Magic Baseline), in three models: the standard three-family oscillation scenario; an extension of the SM with Non-Standard Interactions in matter; and an extension of the SM with one extra light singlet fermion (the so-called 3+1 sterile neutrino model). In the first two cases, the ν_τ detector does not improve the potential of the IDS-NF baseline setup to measure the oscillation parameters or to uncover new physics effects in neutrino oscillations. The reason is that, due to the large mixing in the μ-τ sector, most effects that are present for τ-neutrinos, will have a similar impact also for μ-neutrinos. In these models, the τ-detector could only serve as a tool for resolving parameter degeneracies. This, however, could be also achieved combining the Golden and Disappearance channels and data from two different baselines $L = 4\,000$ km and $L = 7\,500$ km. We must remind that a comparison of the potential of the IDS-NF baseline setup and the same setup with an additional τ-detector to measure the θ_{23}-octant in the standard three-family oscillation model is missing, though (see Ref. [64]).

In the case of the (3+1)-sterile neutrino model, studied in Ref. [4], the availability of the $\nu_\mu \to \nu_\tau$ data using a magnetized ECC has been shown to be extremely important to measure the whole parameter space of the model and, in particular, to study CP-violating phases different from the standard three-family oscillation one, δ.

There may also be a physics case for ν_τ detection if new physics should manifest itself

in the ν_τ detection process, or if non-standard couplings of ν_μ, ν_e to τ leptons or of ν_τ to muons and electrons should exist. However, non-standard contributions to the ν_τ detection process would require a ν_τ detector at a long baseline (e.g. 4 000 km), while non-standard τ and ν_τ production can be most efficiently observed in a ν_τ near detector.
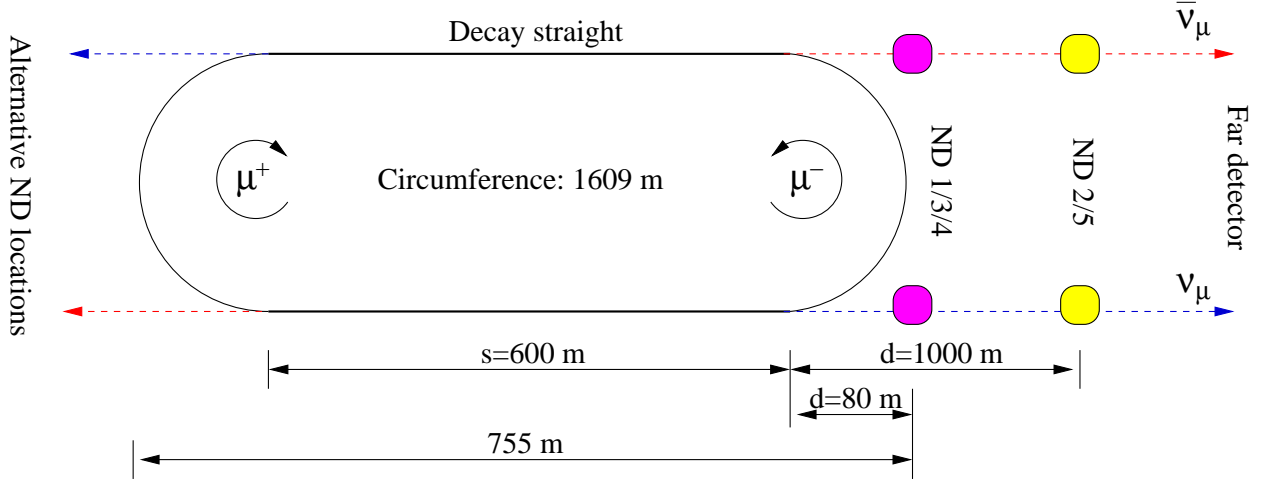
The outcome of this short review is that it is very difficult, at the present stage, to draw a final conclusion on the increase in the Neutrino Factory physics potential to discover new physics if a τ-detector is added to the IDS-NF baseline setup. It is also far from clear which detector technology would be optimal: a good knowledge of the ECC technology will be available only after some years of OPERA data taking; it is not clear if a magnetized ECC, important to increase the ECC statistics, is feasible; the liquid Argon technology has not been studied in detail. Eventually, the technology to be used if a near τ-detector should be built could be completely different from what proposed up to now: due to the high neutrino flux at the near site if exposed to a Neutrino Factory beam, more powerful techniques than what suggested for a large detector could be used, since a smaller detector mass could be sufficient.

In view of these arguments, we suggest that the ECC τ-detector is *not* to be included in the IDS-NF *baseline* setup due to the absence of a compelling physics case and, given the present very preliminary status of the detector design. This does not exclude the option that a ν_τ detector (not necessarily based on the ECC technology) is added to the neutrino factory at a *later stage* of the project if unexpected results from the LHC or from the neutrino factory itself should create a physics case for it.

However, we think it is mandatory to further pursue the study of the potential of such a detector, especially in view of the fact that we do not know what new physics may be out there. Having access to more flavors can only increase the discovery potential of the Neutrino Factory. Notice, eventually, that if θ_{13} results to be large (see solar, atmospheric and MINOS results), part of the statistical problems of the τ-channels become less relevant. At the same time, the main motivation for a Neutrino Factory would become the search for new physics beyond the Standard Model, and therefore the option of an increased flavor sensitivity becomes extremely interesting.

4.5 Relevance of Near Detectors at Nufact

As far as the importance and requirements for near detectors at a neutrino factory are concerned, the questions raised by the *International Design Study for the Neutrino Factory* (IDS-NF) include: What is the potential of near detectors to cancel systematical errors? When do we need a near detector for standard oscillation physics? What (minimal) characteristics do we require, such as technology, number, and sites? What properties do near detectors need for new physics searches? From these questions, we can read off already two obstacles: First of all, one has to address which kind of systematics near detectors should reduce, and second, one has to address what kind of new physics near detectors may help for. In the following, we split the discussion into standard oscillation physics and new physics searches.
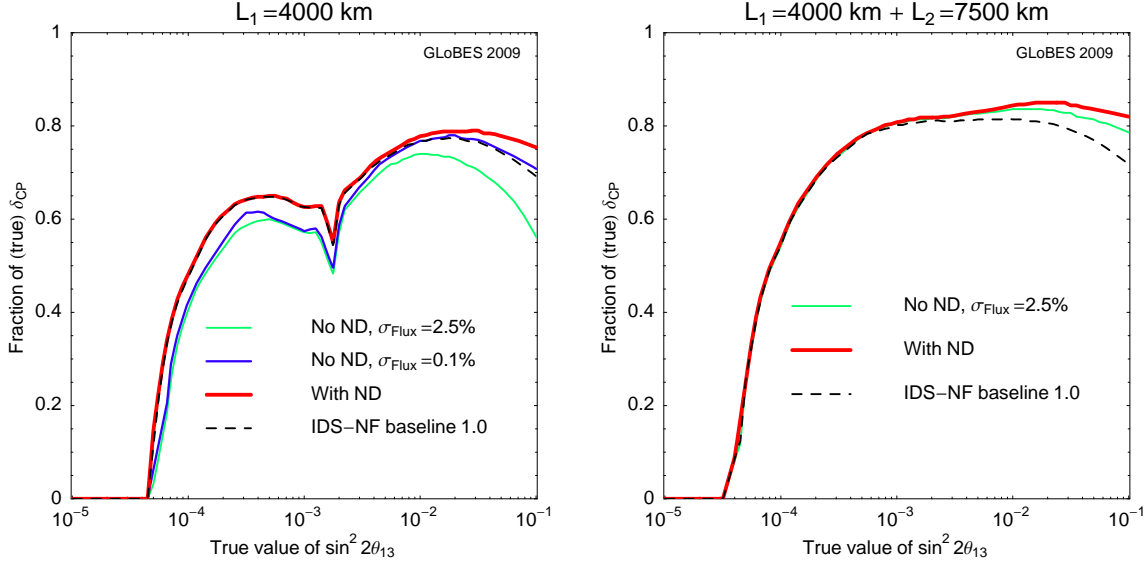
Figure 11: Geometry of the muon storage ring and possible near detector (ND) locations (not to scale). The baseline L is the distance between production point and near detector, *i.e.*, $d \leq L \leq d + s$. Figure taken from Ref. [8].

4.5.1 Near detectors for standard oscillation physics

As it is illustrated in Fig. 11, (at least) two near detectors are required for a neutrino factory if the μ^- and μ^+ circulate in different directions in the ring. For the same reason, charge identification is, in principle, not required, since there are no wrong sign muons produced by oscillations so close to the source. However, for background measurements (such as from charm decays), a magnetic field may be necessary. As it is demonstrated in Ref. [8], the size, location, and geometry of the near detectors hardly matter for standard oscillation physics even in extreme cases of possible near detectors. Because of the high statistics in all energy bins of the near detectors, the physics potential is generally limited by the statistics in the far detector(s). However, note that rare interactions used for flux monitoring, such as inverse muon decays or elastic scattering, may require large enough detectors. A possible near detector design for a neutrino factory is, for instance, discussed in Ref. [40].

As far as the systematics treatment is concerned, the current IDS-NF baseline setup relies on uncorrelated (among all oscillation channels, detectors, and neutrinos-antineutrinos) signal and background normalization errors treating the near detector(s) implicitly, whereas realistic systematics implies particular correlations. For example, the cross section errors are correlated among all channels and detectors measuring the same ν_μ or $\bar{\nu}_\mu$ (inclusive) charged current cross sections, but there may be a shape error, *i.e.*, the errors may uncorrelated among the energy bins. On the other hand, flux errors are correlated among all detectors and channels from the same decays in the same storage ring straight, and they are correlated among different energy bins. In Ref. [8], the systematical errors have been tested which are, in principle, reducible by the use of near detectors. Note that there may be other types of systematics, such as fiducial volume errors, which have not yet been discussed. The refined systematics treatment is illustrated for the CP violation discovery reach in Fig. 12, in comparison to the IDS-NF current parameterization (dashed curves). In the left panel, only one baseline is used. In this case, the near detectors turn out to be very important. In the right panel, the combination of two baselines is shown. The result using the new
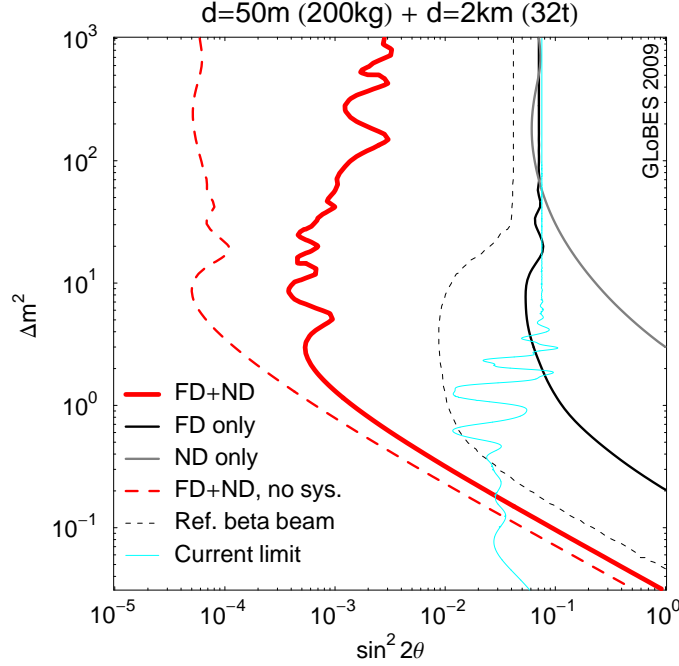
Figure 12: CP violation discovery reach as a function of true $\sin^2 2\theta_{13}$ and the fraction of (true) δ_{CP} for one far detector (left) and two far detectors (right); 3σ CL. Figure taken from Ref. [8].

systematics treatment is already better than the previous one even without near detector, because the cross sections are fully correlated between the two detectors. This means that possible cross section errors cancel. The near detectors improve the result even further.

4.5.2 Near detectors for new physics searches

In order to address the requirements for near detectors for new physics searches, one has to specify which type of new physics. Here we show a number of examples to produce a list of detector requirements which should be as complete as possible. If the new physics originates from heavy mediators, which are integrated out, the new physics can be parameterized in the effective operator picture. The lowest possible effective operators affecting the production, propagation, or detection of neutrinos are dimension six operators, suppressed by v^2/Λ^2 by the new physics scale Λ compared to the SM Higgs VeV v. At tree level, they can be mediated by heavy neutral fermions, leading to a non-unitary mixing matrix after the re-diagonalization and re-normalization of the kinetic terms of the neutrinos (see, *e.g.*, Ref. [6] for a short summary), or by scalar or vector bosons, leading to so-called non-standard interactions (NSI; see, *e.g.*, Ref. [68] for the terminology). A very different type of new physics is the oscillation into light sterile neutrinos, because it may lead to oscillation signatures. We consider near detectors for these three applications. As the common requirement to near detectors compared to standard oscillation physics, the detector mass is very important, because the new physics sensitivity is in many cases limited by the statistics in the near detectors.

The most interesting non-standard interactions for near detectors may be $\epsilon^s_{e\tau}$ and $\epsilon^s_{\mu\tau}$,

Figure 13: Exclusion limit in the $\sin^2 2\theta$-Δm^2 plane for ν_e disappearance into sterile neutrinos from the two detector setup discussed in the main text (thick solid curve, 90% CL, 2 d.o.f.). Figure taken from Ref. [71].

which replace an initial ν_e or ν_μ in the beam by a ν_τ. Since these NSI lead to a zero-distance effect $\propto |\epsilon_{\alpha\tau}|^2$. As illustrated in Ref. [8], the sensitivity to these parameters can be significantly improved in the presence of ν_τ near detectors. If the two effects need to be distinguished, charge identification is required. Assuming that this new physics effect originates from $d = 6$ NSI and that the bounds from charge lepton flavor violation will be strong enough, the bounds from the source effects can be translated into bounds on the matter effect $\epsilon_{\mu\tau}^m$ [52] (see also Ref. [69] for a particular model). In particular models, also other types of NSI at the source may be interesting, such as $\epsilon_{e\mu}^s$ from a Higgs triplet as type-II see-saw mediator [70]. This application relies on excellent charge identification properties of the near detector(s). The above mentioned non-unitarity leads to a particular, fundamental correlation among source, matter, and detector effects. In this case, near detectors improve the measurements in a similar way [6]. Both the NSI and non-unitarity searches have in common that the near detector location only affects statistics, whereas there is no relevant oscillation effect close to the source.

The search for sterile neutrinos is qualitatively different: The location of the near detectors affects the sensitive Δm^2 range. An interesting example is the disappearance of ν_e at short baselines, discussed in Ref. [71]. In this case, the oscillations have to be averaged over the decay straight, which leads to significant effects for near detectors very close to the source (or large Δm^2). In addition, the unknown cross section errors play the same role as the unknown fluxes in the two-detector reactor experiments, such as Double Chooz or Daya Bay. Therefore, a similar approach has been proposed in Ref. [71]: two sets of near detectors

at different (short) baselines, which are sensitive to different Δm^2-ranges, are important for the systematics cancellation of the cross section errors. The result is illustrated in Fig. 13 for $d = 50\,\mathrm{km}$ (ND) and $d = 2\,\mathrm{km}$ (FD), where the thick curve shows the combined sensitivity. If only ND or FD is used (medium thin solid curves), the sensitivity is limited by the knowledge of the cross sections. Obviously, the current bound can be exceeded by two orders of magnitude.

4.5.3 Summary

The requirements/characteristics of near detectors at a neutrino factory can be summarized as follows: For standard oscillation physics, the exact location, size, and geometry of the detectors hardly matters because of the large statistics. Data for the ν_μ and $\bar{\nu}_\mu$ cross sections are already sufficient, because only these two are needed in the far detectors (for a high energy neutrino factory). If the μ^+ and μ^- circulate in different directions in the storage ring(s), at least two near detectors are needed. A magnetic field may be necessary for background measurements.

For nearly all new physics applications, the sizes (masses) of the near detectors are important. Since the size of the detector cannot be arbitrarily increased beyond the opening angle of the beam, the detectors should be as long as possible in order to capture a large portion of the on-axis flux. For new physics searches, all flavors should be measured, and charge identification is mandatory for many applications. For some purposes, such as the short baseline electron neutrino disappearance, more than one set of near detectors may be required. In addition, for any light sterile neutrino oscillation search, the baselines of the near detectors are very important. Energy resolution, on the other hand, is of secondary importance, since the energy resolution is, close to the source, limited by the extension of the decay straight.

In conclusion, near detectors at a neutrino factory are important for both standard oscillation physics and new physics searches. From the physics point of view, however, the requirements, such as size and location, may be driven by new physics searches.

5   Update on betabeam performance

5.1   Baseline scenario optimization

The β-beam concept was first introduced in Ref. [72]. It involves producing a large number of β-unstable ions, accelerating them to some reference energy, and allowing them to decay in the straight section of a storage ring, resulting in a very intense and pure ν_e or $\bar{\nu}_e$ beam. "Golden" sub-leading transitions, $\nu_e \to \nu_\mu$ and $\bar{\nu}_e \to \bar{\nu}_\mu$, can then be measured through muon observation in a distant detector. In the original proposal $^{18}\mathrm{Ne}$ ($^6\mathrm{He}$) ions are accelerated to $\gamma \sim 100$ and stored so that ν_e ($\bar{\nu}_e$) beams are produced and detected at a Mton class water Čerenkov detector located at $L = 130\mathrm{km}$ at the Frejus site. Numerous modifications of this basic setup have been studied, most of them being different combinations of two basic ingredients: the possibility of accelerating the ions to higher γ factors [73, 74], thus increasing the flux and the statistics at the detector, and the possibility of considering the

Element	A/Z	$T_{1/2}$ (s)	Q_β eff (MeV)	Decay Fraction
^{18}Ne	1.8	1.67	3.41	92.1%
			2.37	7.7%
			1.71	0.2%
^{8}B	1.6	0.77	13.92	100%
^{6}He	3.0	0.81	3.51	100%
^{8}Li	2.7	0.83	12.96	100%

Table 2: A/Z, half-life and end-point energies for three β^+-emitters (^{18}Ne and ^{8}B) and two β^--emitters (^{6}He and ^{8}Li). All different β-decay channels for ^{18}Ne are presented.

decay of different ions to produce the neutrino beam. In particular ^{8}B and ^{8}Li have been proposed as alternatives to ^{18}Ne and ^{6}He respectively [75–77]

Here we investigate the physics potential of the $\gamma = 100$ β-Beam option, accessible at the CERN SPS, comparing the different possible choices of ions and baselines. We also take into account the atmospheric background expected at the detector and study the suppression factor of this background required through the bunching of the beam to attain the best sensitivities in the different setups.

In Tab. 2 we show the relevant parameters for the β decay of four ions: ^{18}Ne and ^{6}He, ^{8}Li and ^{8}B. As can be seen, the main difference between the two sets of ions consists in their decay energy: $Q_\beta \sim 3.5$ for ^{18}Ne and ^{6}He and $Q_\beta \sim 12.5$ for ^{8}Li and ^{8}B. Thus, the neutrino beams produced by the decay of the latter set of ions are around 3.5 times more energetic than the ones produced by the former when accelerated to the same γ factor. This also means that, for the oscillation to be on peak, a baseline 3.5 times longer is required to achieve the same L/E value. As a consequence, a suppression of the neutrino flux at the detector of one order of magnitude, since the flux decreases with L^{-2}. For this reason, β-Beams based on ^{8}Li and ^{8}B decays usually suffer from low statistics. This was one of the reasons why ions such as ^{18}Ne and ^{6}He with rather low decay energies were chosen in the original proposal. Despite their statistical limitations, however, ^{8}Li and ^{8}B offer the interesting opportunity to probe higher neutrino energies (with respect to ^{6}He and ^{18}Ne beams) using the maximum γ factor achievable at the existing facilities. The higher energies accessible translate in stronger matter effects and generally higher sensitivity to the neutrino mass hierarchy through them.

A key factor in the determination of the best ion candidates is the achievable number of decays per year for each ion. This factor is at present extremely uncertain. For ^{18}Ne and ^{6}He "standard" fluxes of 1.1×10^{18} and 2.9×10^{18} useful decays per year are usually assumed. These fluxes would grant the $\gamma = 100$ β-Beam proposal enough sensitivity to compete with similar Super-Beam facilities. Preliminary studies show that this requirement should be achievable for ^{6}He ions (the estimations actually yield a flux somewhat larger, of 3.18×10^{18} useful decays per year). In the case of ^{18}Ne, on the other hand, the production of an intense flux is much more challenging and the present estimates fall two orders of magnitude short of the mark, yielding a flux of 4.64×10^{16} useful decays per year. We will present results for both assumptions of the fluxes for ^{18}Ne and ^{6}He, the nominal one and that achievable
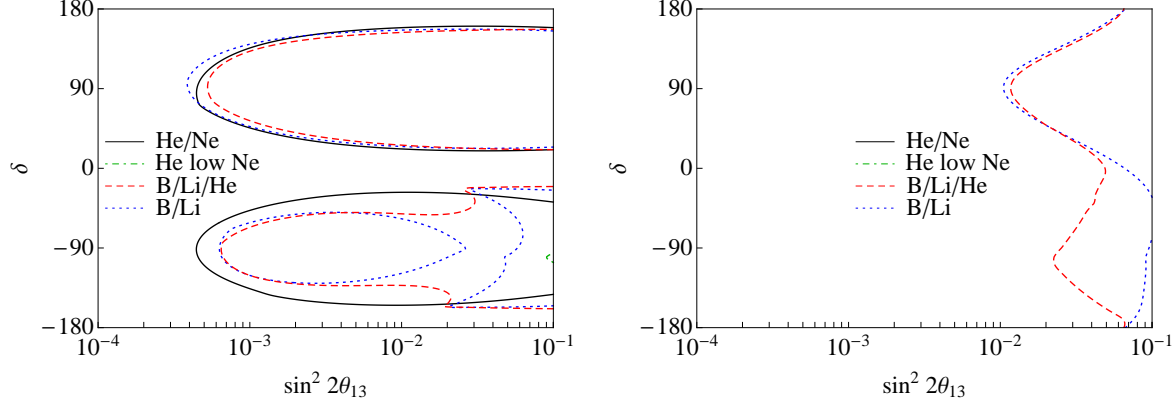
with present studies. A similar analysis of the achievable fluxes for ^{8}Li and ^{8}B is only in its very early stages. Assuming that the two ions can be produced with the rates described in [75] a preliminary estimate of its fluxes after the acceleration up to $\gamma = 100$ through the SPS yielded 3.49×10^{18} and 7.56×10^{18} useful decays per year for ^{8}B and ^{8}Li, respectively. We will evaluate the sensitivities achievable with neutrino beams based on the decays of ^{8}Li and ^{8}B assuming these production fluxes. However, the extraction of this intense ^{8}B fluxes could be challenging, since B is known to be very reactive and difficult to release.

The choice of the baseline should match the neutrino energy, since neutrino flavour change oscillates with L/E. Too short a baseline will not allow oscillations to develop and a baseline much larger than the one matching the first oscillation peak will reduce unnecessarily the statistics at the detector due to the beam divergence as L^{-2}. There are two sites capable of housing the Mton class water Cerenkov detector proposed to observe the neutrino beam produced at CERN and that match the baseline requirements. The shorter baseline is 130 Km and matches the CERN to Frejus distance. It is suited to observe the first oscillation peak of neutrinos from ^{18}Ne and ^{6}He decays accelerated to $\gamma = 100$, and it was the baseline suggested in the original β-Beam proposal. A longer baseline of 650 Km would correspond to the CERN to Canfranc distance and would roughly match the first oscillation peak of neutrinos from ^{8}Li and ^{8}B decays accelerated to $\gamma = 100$. Oscillations of neutrinos from ^{18}Ne and ^{6}He could also be observed at this baseline at the second peak for $\gamma = 100$ or at the first peak for $\gamma = 350$ (achievable with a refurbished SPS [73]).

With the four ion candidates and two baselines available we have explored the sensitivities to the unknown parameters of four possible β-Beam setups:

- 1. The "standard" setup with neutrinos from ^{18}Ne and ^{6}He decays accelerated to $\gamma = 100$. The baseline is $L = 130$ Km and the fluxes are given by 1.1×10^{18} and 2.9×10^{18} useful decays per year for ^{18}Ne and ^{6}He, respectively. We assumed a 5 year run with each ion. This setup is represented by the black solid line in Fig 14.

- 2. The same as setup 1 but with the estimated fluxes of 4.64×10^{16} and 3.18×10^{18} useful decays per yer for ^{18}Ne and ^{6}He, respectively. This is depicted by the green dotdashed line in Fig 14.

- 3. A setup based in ^{8}Li and ^{8}B decays accelerated to $\gamma = 100$. The baseline is $L = 650$ Km and the fluxes 3.49×10^{18} and 7.56×10^{18} useful decays per year for ^{8}B and ^{8}Li, respectively. We assumed a 5 year run with each ion. This setup is represented by the blue dotted line in Fig 14.

- 4. A setup based in ^{8}Li, ^{8}B and ^{6}He decays accelerated to $\gamma = 100$. The baseline is $L = 650$ Km; the same fluxes as for setups 2 and 3 were assumed. We assumed a 5, 3 and 2 year run with ^{8}B, ^{8}Li and ^{6}He, respectively. This setup is represented by the red dashed line in Fig 14.

The expected efficiencies and beam-induced backgrounds of the detector when exposed to the considered beams has been added as migration matrices extracted from Ref. [74]. In all the simulations the following best fit values and 1σ errors for the known oscillation parameters were assumed: $\Delta m_{21}^2 = (8.0 \pm 0.3) \times 10^{-5}$ eV^2, $\Delta m_{31}^2 = (2.6 \pm 0.1) \times 10^{-3}$ eV^2,

Figure 14: Comparison of the $3\,\sigma$ discovery potential of different β-Beam setups to leptonic CP-violation (left panel) and the mass hierarchy (right panel). Solid, dotdashed, dotted and dashed lines correspond to the setups, 1, 2, 3 and 4 described in the text, respectively. Taken from Ref. [9].

$\theta_{12} = 33.0°\pm1.3°$ and $\theta_{23} = 45.0°\pm4.5°$. These parameters were marginalized over to present the final curves. The background caused by atmospheric neutrinos in the detector was neglected in this section but will be discussed in detail in the next section. The evaluation of the performance of the detector made use of the GLoBES software [24, 25].

The expected CP discovery potential (defined as the values of θ_{13} and δ that would allow to discard at 3σ the CP-conserving values $\delta = 0$ and $\delta = \pi$) of the four setups considered is presented in the left panel of Fig 14. The discovery potential down to the smallest values of θ_{13} corresponds to setup 1, since the shorter baseline guarantees higher statistics. However, taking into account the very low fluxes estimated for ^{18}Ne in setup 2, the sensitivity to CP-violation is lost. Setup 3, based on ^{8}B and ^{8}Li decays has a smaller statistics and worse sensitivity for small values of θ_{13}. Moreover, the stronger matter effects present at these higher energies and baseline can mimic true CP-violation and lead to degeneracies that translate into the loss of sensitivity for negative values of δ around $\sin^2 2\theta_{13} = 3 \times 10^{-2}$. In order to alleviate this degeneracy problem we introduced setup 4: the combination of information at the first oscillation peak from ^{8}B and ^{8}Li beams with that from a ^{6}He beam at the second oscillation peak is enough to solve the sign degeneracies and fill in the gap in sensitivity for negative values of δ [76].

The term in the oscillation probability that provides the sensitivity to CP-violation is suppressed by $\sin 2\theta_{13}$ and $\Delta m_{21}^2 L/E$ and has to compete with a δ-independent term suppressed by $\sin^2 2\theta_{13}$. The sensitivity to CP-violation thus decreases for the largest values of θ_{13}, where the δ-independent term dominates. However, in setups 3 and 4 the value of L/E is larger for the lower energy bins than in setup 1 and, thus, their sensitivity to CP-violation outperforms that of setup 1 for large values of θ_{13} even if their statistics is lower. It should also be remarked that the expected statistics in the detector strongly depends of the assumed value of the cross section which, at very low energies below 1 GeV, is plagued by nuclear effects uncertainties and different computations can differ up to a factor two, leading to very different estimations of the sensitivity for the lower energy setups 1 and 2. The cross section assumed here is particularly optimistic at these low energies, which

emphasizes the statistics difference between setup 1 and setups 3 and 4, allowing it to reach smaller values of θ_{13}.

The expected discovery potential to a normal mass hierarchy, defined as the values of θ_{13} and δ that would allow to discard an inverted hierarchy at 3σ, of the four setups considered is presented in the right panel of Fig 14. Notice that only setups 3 and 4 show some sensitivity to mass hierarchy. Setups 1 and 2 have too small matter effects due to the low energy of the beam and the shorter baseline to be able to measure the mass hierarchy by themselves. Nevertheless, some sensitivity to the mass hierarchy could be gained when combining their information with atmospheric neutrino oscillations measured at the detector [78]. The better sensitivity of setup 4 with respect to setup 3 for negative values of δ is again due to the complementarity of the information on the oscillation probability of ^{6}He at the second oscillation peak that allows to break degeneracies when combined with ^{8}Li and ^{8}B at the first peak [76].
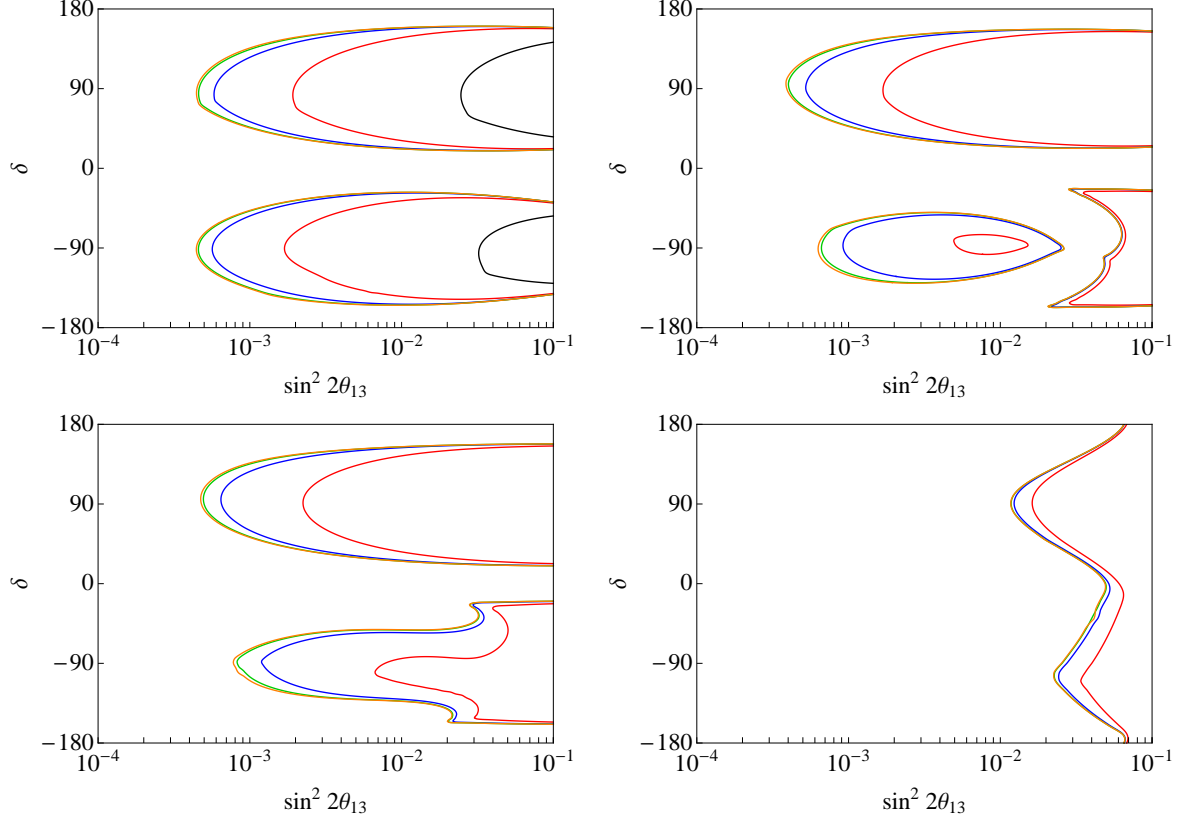
We conclude that the setups 3 and 4 based on ^{8}Li and ^{8}B decays outperform the standard setup 1 based on ^{18}Ne and ^{6}He decays for values of $\sin^2 2\theta_{13} > 2 \times 10^{-2}$, providing a better sensitivity to CP-violation and to the mass hierarchy. For small values of θ_{13}, setup 1, with its better statistics, is the better option. However, if it turns out that the present estimation of the achievable ^{18}Ne fluxes cannot be improved, all the sensitivity to CP-violation is lost (setup 2) and alternative setups based on ^{8}Li and ^{8}B decays would remain the only option.

5.2   The atmospheric neutrino background

One of the main sources of background that can spoil the β-Beam sensitivity is the background from atmospheric neutrinos. This background can be reduced by imposing angular cuts in the direction of the beam. The typical scattering angle of the lepton produced in CC interactions with respect to the incident neutrino is $\sim \sqrt{1/E}$. We have evaluated the expected number of muon neutrinos arriving within a solid angle $\sim \sqrt{1/E}$ in the beam direction for the different energy beams and studied its impact on the sensitivities. Even after imposing this directional cut the background level dominates the expected signal and an additional cut must be imposed to reduce it to acceptable levels. This can be achieved by accumulating the signal in small bunches so as to use timing information to reduce the constant atmospheric background. Previous analysis showed that for the standard setup the decaying ions must be accumulated in very small bunches occupying just a $\sim 10^{-3}$ fraction of the storage ring so as to achieve a 10^{-3} suppression factor of the background. Since the atmospheric neutrino background decreases with the energy as $\sim E^{-2}$, for the setups considered here based on ^{8}Li and ^{8}B decays with ~ 3.5 times higher energy, an order of magnitude less atmospheric background can be expected at the detector. We studied whether this allows to relax the stringent $\sim 10^{-3}$ bunching required on the signal. Notice that the achievable ion flux is strongly affected by this strong requirement and a relaxation of this value could allow an increase in statistics.

In Fig. 15 we show the dependence on the background suppression factor of the 3σ discovery potential to leptonic CP-violation (left panels) and the mass hierarchy (right panels). The lines correspond to no atmospheric background (orange) and to suppression factors of 10^{-4} (green), 10^{-3} (blue) and 10^{-2} (red). The upper panels correspond to setup 1 (left) and 3 (right), respectively. We can see from these two plots that there is almost no

Figure 15: Dependence on the background suppression factor of the the $3\,\sigma$ discovery potential to leptonic CP-violation for setup 1 (upper left), setup 3 (upper right) and setup 4 (bottom left). The bottom right panel represents the sensitivity to the mass hierarchy for setup 4. The lines correspond to no atmospheric background (orange) and to suppression factors of 10^{-4} (green), 10^{-3} (blue) and 10^{-2} (red). Taken from Ref. [9].

difference between the sensitivity with no atmospheric background (orange line) and with a 10^{-4} background (green line). The atmospheric background thus becomes negligible if a 10^{-4} suppression is achieved. The sensitivities for the 10^{-3} suppression case (blue lines) are only slightly worse than those for 10^{-4}. Thus, 10^{-3} seems the goal that should be achieved in order to exploit the full potential of the β-Beam. However, it can be seen that, whilts setup 1 have a CP discovery potential that is independent on the sign of the CP-violating phase, setup 3 (that is more sensible to matter effects) suffers from degeneracies for negative δ. This is cured by the addition of a component of ^{6}He beam in setup 4 that, combined with the two high-Q beams solve the sign degeneracy and restore symmetry between positive and negative δ values (lower panel, right). The sensitivity to the mass hierarchy in setup 4 can be seen in lower panel (right) as a function of the suppression factor. Notice that, for all setups, the CP discovery potential is strongly degraded for a suppression factor of 10^{-2}.

We conclude that in all the setups studied a background suppression of $\sim 10^{-3}$ is required to achieve the full sensitivity of the β-Beam. The fact that the higher energy beams provided by ^{8}Li and ^{8}B decays require the same background suppression than those based on ^{18}Ne and ^{6}He is the non-trivial consequence of many factors.

37

The suppression of the signal for the high-Q beam is not fully compensated by the higher cross section at higher energies (more than a factor 3.5 larger since the cross section grows faster than linearly at those energies) and by the higher flux assumed here for ^{8}B and ^{8}Li, around three times larger. Eventually, the efficiency of the detector gets degraded at high energies, since water Čerenkov detectors are not optimal beyond the quasi-elastic regime of the cross section. In particular, following Ref. [74], we find the efficiencies to be around more than a factor two smaller for the higher Q ions than for ^{18}Ne and ^{6}He. This means that the signal/background fraction remains similar in all scenarios and a suppression factor $\sim 10^{-3}$ is always required to achieve the full β-Beam potential.

5.3   Greenfield scenario optimization: two baseline betabeam

It is well-known that for $L \sim 7000$ km the density encountered by the (anti)neutrinos allows for a resonant enhancement in the probability when $E_\nu \sim 6$ GeV if the mass hierarchy is normal (inverted). Therefore, ^{8}B and ^{8}Li turn out to be the best candidates to determine the mass hierarchy, as their end point energies are much higher than those of the "standard" ions, ^{6}He and ^{18}Ne.

However, another detector at a short baseline is needed in order to probe CP-violation, as δ cannot be measured at the magic baseline. For neutrinos coming from ^{6}He and ^{18}Ne decays at $\gamma = 350$, the mean neutrino energy of $E_0\gamma \sim 1.2$ GeV translates into an on-peak baseline of $L = 618$ km, while for ^{8}B and ^{8}Li this baseline would be $L \sim 1500 - 2000$ km. As the flux is proportional to L^{-2}, ^{6}He and ^{18}Ne turn out to be the best candidates to probe CP-violation.

The original design of the storage ring proposed in [72] must be modified when the boost factor is increased up to $\gamma = 350$. If we use LHC dipolar magnets to bend the ions, and keeping the straight sections untouched, the useful fraction of ion decays for this ring (also called "livetime") would be[5] $l = 0.28$, the total length being $L_r = 8974$ m. The tilt angle needed to aim at the near detector is $\vartheta = 3°$: this means that the maximum depth of the far end of the ring is $d = 197$ m. However, the tilt angle to aim at $L = 7000$ km is $\vartheta = 34.5°$. In this case, the ring would reach a depth of $d = 2132$ m, something well beyond any realistic possibility.

Note that with the refurbished SPS (SPS+) the ^{8}B and ^{8}Li ions could be accelerated up to $\gamma = 650$ and $\gamma = 390$, respectively. Due to the resonance, this 10% increase in the γ factor for ^{8}Li produces an increase of a 40% in the number of antineutrino events at the detector. Therefore, we can reduce the livetime $l = 0.6 \times 0.28 \sim 0.17$ by reducing the straight section of the ring to $L = 998$ m, and the physics reach of the setup will remain practically unaffected. This ring would be almost 1 Km less deep than the one described above, $d = 1282$ m.

We make the following choices for our detectors: (1) Since CP measurements are better at lower energies, it is preferable to have a detector with low threshold and good energy resolution. We opt for a water Čerenkov detector with 500 kton fiducial mass (as in Refs. [73, 74]). This detector could be hosted at Canfranc, for example, at a distance of 650 km from the β-Beam at CERN; (2) Higher energy neutrinos from highly boosted ^{8}B and ^{8}Li ions will

---

[5]$l_{\text{racetrack}} = \frac{L_{\text{straight}}}{2L_{\text{straight}} + 2\pi R}$

be sent to the far detector. We prefer thus to choose a 50 kton magnetized iron detector for the magic baseline: the ICAL@INO detector in India [79], located at a distance of 7152 km, which will soon go under construction.

To simulate the response of the water Čerenkov detector we use the migration matrices given in [73], while for the iron detector, we follow the efficiencies and backgrounds derived in [40] for the Neutrino Factory (NF) fluxes. Notice that this is a very conservative assumption, since for a β-Beam charge identification is not mandatory, unlike in the NF. Therefore, the charge ID capability of the detector could be used to further reduce the background. Finally, the performance of the iron detector is affected by large uncertainties at energies around $1-5$ GeV. However, we need this detector only to observe the resonance in the probability which takes place around $6-7$ GeV, so these uncertainties will practically have no effect at all in the performance of our setup.

Preliminary studies on the ion production rates show that these could be enhanced in the near future. Therefore, as β-Beams are facilities under study for construction in the next two decades, we will assume that 10^{19} ions per year can be stored into the ring, for all ion species [80], with a livetime $l = 0.28$ for the ring aiming at the 650 Km baseline and $l = 0.6 \times 0.28$ for the ring aiming at the magic baseline. For ^{6}He and ^{18}Ne beams, this means that we are considering $\sim 3 \times 10^{18}$ useful decays per year aiming at the 650 Km detector. This choice corresponds to the nominal flux for ^{6}He ions and roughly twice the nominal flux for ^{18}Ne ions[6]. For the four ions setup proposed in Ref. [10], a runtime with each ion species of 2.5 years is considered.

We present in Fig. 16 the comparison of the performance of our setup with the IDS Neutrino Factory design [1] (with 25 GeV muons stored in two racetrack rings aiming at two 50 Kton magnetized iron detectors of the MIND-type located at $L = 4000$ Km and $L = 7500$, respectively, with 5×10^{20} useful muon decays per year aiming at each detector) and the one-baseline β-Beam set-up proposed in [73, 74], where neutrino beams produced by ^{18}Ne and ^{6}He decays accelerated to $\gamma = 350$ are detected in a 500 kton water Čerenkov detector located at 650 km. In both setups, five years of data taking with neutrinos and anti-neutrinos are considered.
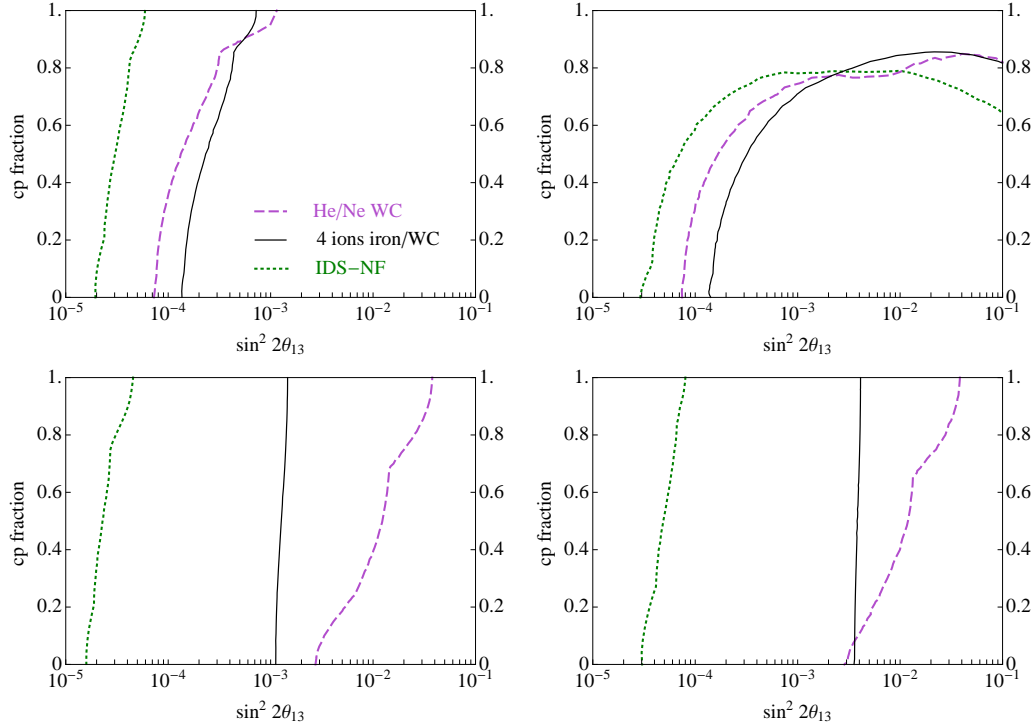
We have considered 2.5% and 5% systematic errors on the signal and on the beam-induced background, respectively. They have been included as "pulls" in the statistical χ^2 analysis. The following 1σ errors for the oscillation parameters were also considered: $\delta\theta_{12} = 1\%$, $\delta\theta_{23} = 5\%$, $\delta\Delta m_{21}^2 = 1\%$ and $\Delta m_{31}^2 = 2\%$. Eventually, an error $\delta A = 5\%$ has been considered for the Earth density given by the PREM model [41, 42]. Marginalization over these parameters has been performed for all observables. The Globes 3.0 [24, 25] software was used to perform the numerical analysis.

We quantify the physics reach of the experiments in terms of three different performance indicators:

1. The $\sin^2 2\theta_{13}$ discovery reach: This is the minimum true value of $\sin^2 2\theta_{13}$ for which the experiment can rule out at the 1 d.o.f. 3σ the value $\sin^2 2\theta_{13} = 0$ in the fit, after marginalizing over all the other parameters.
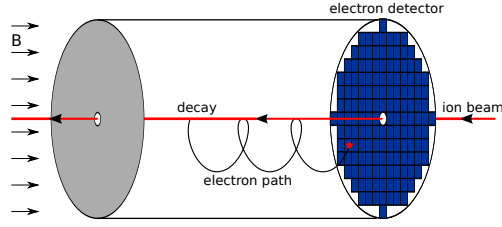
---

[6]Notice that, as it was stressed in Sect. 5.1, at present a flux of only 4.6×10^{16} useful ^{18}Ne ion decays are achievable.

Figure 16: Comparison of our proposed set-up (black solid lines) with the IDS Neutrino Factory baseline design (green dotted lines) and the high γ β-Beam set-up from [73,74]. The upper left hand panel shows $\sin^2 2\theta_{13}$ discovery reach, the upper right hand panels shows the CP violation reach, and the lower panels show the mass hierarchy discovery reach for normal (left panel) and inverted (right pannel) hierarchy. All sensitivities are presented as a function of the fraction of the values of δ for which they can be discovered. Taken from Ref. [10].

2. The CP-violation reach: This is the range of δ as a function of $\sin^2 2\theta_{13}$ which can rule out no CP-violation ($\delta = 0$ and $180°$) at the 1 d.o.f. 3σ, after marginalizing over all the other parameters.

3. The $sgn(\Delta m_{31}^2)$ reach in $\sin^2 2\theta_{13}$: This is defined as the limiting value of $\sin^2 2\theta_{13}$ for which the wrong hierarchy can be eliminated at 3σ.

From Fig. 16 it is clear that the facility with sensitivity to the different observables down to smallest values of $\sin^2 2\theta_{13}$ is the Neutrino Factory. This can be understood from the much larger fluxes assumed for the IDS setup: 5×10^{20} useful muon decays per year and per baseline to be compared to the 3×10^{18} assumed for the β-Beams. On the other hand, the high energy of the Neutrino Factory beams implies a very small value of L/E_ν. This translates into a stronger suppression of the CP-violating term of the oscillation probability with respect to the one suppressed by two powers of θ_{13} for large values of this parameter. Therefore, the CP discovery potential of β-Beams outperforms that of the Neutrino Factory in Fig. 16 when $\sin^2 2\theta_{13} > 10^{-3}$. Since this large value of $\sin^2 2\theta_{13}$ also guarantees a discovery of the mass hierarchy and $\sin^2 2\theta_{13}$ regardless of the value of δ, this makes β-Beams the best option when $\sin^2 2\theta_{13} > 10^{-3}$. Furthermore, even if the statistics at the

Figure 17: Measuring absolute neutrino mass with ion beams. The ion beam enters an evacuated cavity whose back wall holds an electron detector. Each ejected electron follows a helical trajectory. Electrons moving in the backward direction in the laboratory frame are counted by the detector. Taken from Ref. [11].

near detector is reduced by half in our proposal compared to the one in Ref. [73, 74] (we are running only 2.5 years with ^{6}He and ^{18}Ne beams, instead of five years), the CP-discovery potential for $\sin^2 2\theta_{13} > 10^{-3}$ is better in the two-baseline set-up due to the lifting of the degeneracies that can mimic CP-conservation when combining the information from the two detectors.

5.4   Measuring absolute neutrino mass with Beta Beams

In Ref. [11] a method has be proposed to measure the neutrino mass kinematically using beams of ions which undergo beta decay. The idea is to tune the ion beam momentum so that in most decays, the electron is forward moving with respect to the beam, and only in decays near the endpoint is the electron moving backwards, see Fig. 17. Then, by counting the backward moving electrons one can observe the effect of neutrino mass on the beta spectrum close to the endpoint. There are stringent requirements of the proposed setup in order to exceed the sensitivity of 0.2 eV of the latest generation of Tritium and Rhenium decay experiments. A crucial question is whether it will be possible to accelerate enough ions within reasonable time such that of order $10^{18} - 10^{20}$ decays can be observed. This issue is also related to the identification of a suitable ion with a low enough Q-value (in order to maximize the effect of the neutrino mass), and a small enough half life (in order to have a high enough decay rate).

As an example, for a very low Q-value of 2 keV, one needs 4×10^{16} decays to obtain the KATRIN sensitivity of 0.2 eV, while 10^{19} decays will allow for a m_ν^{eff} measurement at 0.04 eV. On the other hand, if no suitable ion with such a low Q-value can be identified the requirements on the total number of decays increases drastically: for $Q = 4\,(8)$ keV the 0.2 eV sensitivity is reached for $5 \times 10^{17}\,(8 \times 10^{18})$ decays, respectively. The sensitivity goal of $m_\nu^{\text{eff}} < 0.04$ eV, which will separate the normal and inverted neutrino mass hierarchy regions, requires in excess of 10^{19} counts across the run of the experiment together with a Q-value of 2 keV. Further requirements are control over ion momentum with a precision better than $\delta p / p < 10^{-5}$, and separation of forward and backward going electrons with very good precision.

5.5 Progress in monochromatic betabeams

The next generation of long baseline neutrino oscillation experiments will aim at determining the unknown mixing angle θ_{13}, the type of neutrino mass hierarchy and CP-violation. We discuss the separation of these properties by means of the energy dependence of the oscillation probability and we consider a hybrid setup which combines the electron capture and the β^+ decay from the same radioactive ion with the same boost. We study the CP discovery potential for different boosts and baselines. We conclude that the combination of the two decay channels, with different neutrino energies in a single experiment, achieves remarkable results.

5.5.1 Energy Dependence

The magnitude of the T-violating and CP-violating interference in neutrino oscillation probabilities is directly proportional to $\sin\theta_{13}$ [81–85]. CP-violation can be observed either by an Asymmetry between neutrinos and antineutrinos and/or by Energy Dependence in the neutrino channel. In the last case, the CP phase δ plays the role of a phase shift in the interference pattern between the atmospheric and solar amplitudes for the appearance oscillation probability. This result is a consequence [85] of the assumptions of CPT-invariance and No Absorptive part in the oscillation amplitude: the Hermitian character of the Hamiltonian responsible of the time evolution says that the CP-odd=T-odd probability $P(\nu_e \to \nu_\mu) - P(\bar{\nu}_e \to \bar{\nu}_\mu)$ is an odd function of time, i.e., an odd function of the baseline L. In vacuum neutrino oscillations for relativistic neutrinos, the oscillation phase depends on the ratio L/E, and then the CP-odd term becomes an odd function of the energy E for fixed L. With the same reasoning, the CP-even terms are even functions of the energy E in the oscillation probability. In this way, Energy Dependence in the appearance oscillation probability is able to disentangle CP-even and CP-odd terms. One can check these properties in the explicit expression for the suppressed appearance probability for neutrinos in vacuum oscillations.

This result suggests the idea of disentangling δ from $|U_{e3}|$ without a need of comparing neutrino and antineutrino events, which have different beam systematics and different cross sections in the detector: either monochromatic neutrino beams with different boosts or a combination of channels with different neutrino energies in the same boost are able of separating the CP-violating phase.

Due to neutrino propagation through the Earth, matter effects can "fake" CP-violation in the sense that the presence of matter affects neutrino and antineutrino oscillations in a different way. It is not easy to disentangle matter effects from CP-violation since there is the so-called "mass hierarchy degeneracy", which swaps the effect of matter for neutrino and antineutrino oscillation according to the sign of Δm_{31}^2. The energy dependence of the $\nu_e \to \nu_\mu$ oscillation probability, in presence of matter effects, can be studied [61, 86] observing that the energy dependence induced by the presence of matter is different in the three terms T_{atm}, T_{sol} and in the interference T_{int} and, in fact, different from the energy dependence associated with the CP-even versus the CP-odd separation. On the other hand, the mass hierarchy degeneracy in vacuum is now removed because T_{atm} and T_{int} are now changing under the change of sign of Δm_{31}^2, although T_{sol} remains the same. All in all,

we observe the virtues of studying the neutrino appearance probability as a function of the neutrino energy.

From the current discovery phase of θ_{13}, next generation experiments will hence aim at precision measurements of the $\nu_e \rightarrow \nu_\mu$ oscillation probability. This will require large underground detectors coupled to more intense and pure neutrino beams. These aspects are being studied within the LAGUNA and EURONu design studies. The knowledge on the possible values of θ_{13} is a necessary input to best optimize the search for CP-violation in the leptonic sector.

A sister approach to the beta-beam is to use the neutrinos sourced from ions that decay mainly through electron capture (EC) [87,88]. We discuss here a hybrid [12] of the EC and β^+ approaches. By selecting a nuclide with $Q_{EC} \sim 4$ MeV, we can make use of neutrinos from an electron capture spike and β^+ continuous spectrum simultaneously. Assuming a detector with low energy threshold, the use of such ions allows one to exploit the information from the first and second oscillation maxima with a single beam. The use of the hybrid approach makes it possible to use a monochromatic beam at higher energies and a beta-beam at lower energies. The need for good neutrino energy resolution at the higher energies will therefore be less crucial than for high-γ beta-beam scenarios.

5.5.2 Combined EC plus β^+ Beam

In this section we discuss the results of the idea [12] of the beta-beam and electron capture hybrid approach, as applied to the decay of Yterbium ($^{156}_{70}$Yb). We simulate appearance experiments divided into four setups with the following characteristics:
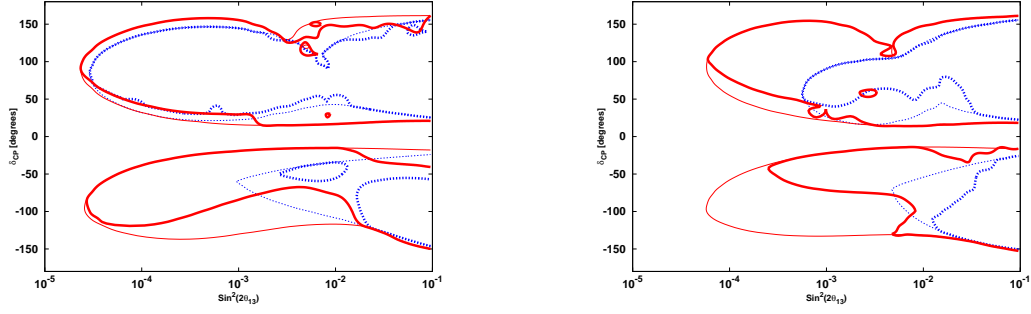
1. 50 kton detector (LAr or TASD) with 2×10^{18} ions/yr

   - **Setup I**: CERN-Frejus (130 km) and $\gamma = 166$
   - **Setup II**: CERN-Canfranc or Gran Sasso (650 km) and $\gamma = 166$
   - **Setup III**: CERN-Canfranc or Gran Sasso (650 km) and $\gamma = 369$
   - **Setup IV**: CERN-Boulby (1050 km) and $\gamma = 369$

2. 0.5 Mton water-Čerenkov detector with 2×10^{18} ions/yr

   - **Setup III-WC**: CERN-Canfranc or Gran Sasso (650 km) and $\gamma = 369$
   - **Setup IV-WC**: CERN-Boulby (1050 km) and $\gamma = 369$

Setups I and II correspond to present SPS energies for the boost, whereas III(-WC) and IV(-WC) need an upgraded SPS with proton energy 1 TeV.
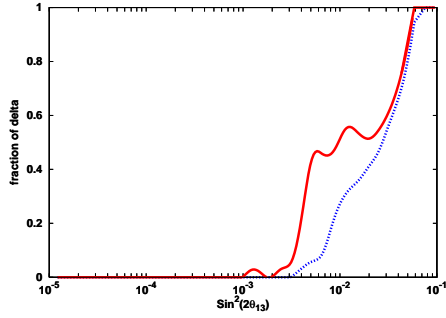
The best results are obtained for the setups with large Water Cerenkov detector. The plots in Fig. (18) represent the CP discovery potential for the setups with intermediate and larger baseline for high boost and large detector. Note that the 650 km baseline has a significantly better reach for CP violation at negative values of δ than the Boulby baseline.

The plot in Fig. (19) represent the fraction of the CP phase δ for which the neutrino mass hierarchy can be determined for setup IV-WC. The Boulby baseline, with its larger matter effect, is better for the determination of the mass hierarchy.

Figure 18: CP-violation discovery potential at 99% CL for setup III-WC (left panel) and IV-WC (right panel). In each case, we present the results for the beta-beam only (blue dotted lines) and the combination with the electron capture result (red solid lines), both without (thin lines) and with (thick lines) taking the hierarchy degeneracy into account. Taken from Ref. [12].

Figure 19: Fraction of δ for which the neutrino mass hierarchy can be determined at 99% CL for setup IV-WC. We present the results for the beta-beam only (blue dotted lines) and the combination with the electron capture result (red solid lines). Taken from Ref. [12].

The principle of energy dependence to separate out the CP-even and CP-odd contributions to the neutrino oscillation probability works. The combined channels result in a good resolution on the intrinsic degeneracy, and on CP phase sensitivity. While the SPS upgrade is crucial for a better sensitivity to CP violation, it is so provided it is accompanied by an appropriate baseline of 650 km. The setups with the larger baseline provide a better determination of the hierarchy and still a good reach to CP violation for negative δ, even if the mass ordering is unknown. The main conclusion is that the combined experiment achieves remarkable results. Up to now, past results on the production rate of these proton-rich ions are of the same order as for light ions. It would be desirable to study the expectactions in the future radioactive ion facility.

6 Update of the SPL super-beam physics potential

The simulations developed so far for the SPL-Fréjus Super Beam foresee the use of a liquid mercury-jet target in order to efficiently dissipate the heat produced by the 4 MW incoming proton beam from the HP-SPL [89]. Due to the low energy of incoming protons (4 GeV) the emission angle of secondary pions is large enough to force the use of a horn-embedded target in order to preserve a good collection efficiency. It should be noted that recent results from the MERIT collaboration [90] support the importance of a high magnetic field to mitigate the explosion of the mercury jet. This can be achieved by using superconducting solenoids

for the capturing system. This solution is acceptable for the neutrino factory design but not for a Super Beam due to the lack of charge discrimination. In the current scenario the focusing system is composed of two concentric magnetic horns. Recent efforts [13, 91] have then been focused on the study of a solid target option which would greatly simplify the problem of the integration of the target and the focusing system and more importantly would avoid the difficult issues related to the mercury jet handling in a magnetic field free region. The impact of using a solid target has been studied in terms of both technical aspects (the power dissipation in the target) and physics performance related aspects (pion and kaon yields, pion collection efficiency with a long target, ν fluxes and sensitivity to δ_{CP} and θ_{13}).

A graphite target was chosen since it is already an adopted technology in current experiments. As a first attempt the graphite (ρ=1.85 gcm^{-3}) target was chosen to have the same radius of the previos mercury target (0.75 cm) and a length of 78 cm (instead of 30 cm for mercury) to roughly preserve the prescription of having $\sim 2\lambda_I$ of material. The power released in the target has been estimated using FLUKA2008.3[7] and GEANT4. At 4 GeV the deposited power is $\sim$ 250 kW for the graphite target and 700 kW for the mercury one. The evolution of absolute particle yields for different particles ($K^{\pm}$, $K^0(\bar{K}^0)$, $\pi^{\pm}$, n) has been studied as a function of $E_k(p)$ from 2 to 10 GeV with FLUKA working at constant power. The pion yield for the mercury target is reasonably stable with energy at $\sim 3 \cdot 10^{15}$ π^+/s and $2.5 \cdot 10^{15}$ π^-/s. The graphite target gives a rather flat rate of $\sim 2.5 \cdot 10^{15}$ π^-/s while the larger π^+ flux decreases from $\sim$ 4.5 to $\sim 3 \cdot 10^{15}$ π^+/s at 10 GeV. The most striking difference between the two targets is the neutron yield which is about a factor $\times$ 15 larger in the case of mercury. A reduced neutron flux is highly beneficial in terms of aluminum radiation damage. At 5 GeV a structure occurs in the yields of π^- and neutrons. At this energy the matching of different inelastic hadron-nucleus production models (Glauber-Gribov multiple scattering + GINC model below and PEANUT model above) occurs. A similar structure used to be observed in kaon spectra at 3.5 GeV in FLUKA2002.4 [89]. Neutrino fluxes have been computed with GEANT3 and the standard horn for kinetic energies of 2.2,3.5,4.5 and 8.0 GeV for both both positive and negative focusing [13].

The obtained fluxes reflects the pion yields and thus graphite fluxes result to be of the same order or even larger than the ones obtained with graphite depending on energy. On the other hand a quite higher contamination of $\bar{\nu}$ in the neutrino beam and particularly ν in the $\bar{\nu}$ beam is observed due to the fact that with the standard horn many wrong charge pion emerging in the downstream part of the target and at low angles are not effectively defocused. The $\sin^2 2\theta_{13}$ sensitivity curves (at 3σ C.L.) have been re-evaluated after the substitution of the standard mercury target with the graphite one. A worsening of the limit with graphite in the $\delta_{CP} < \pi$ region which is driven by $\bar{\nu}$ running (π^- focusing) has been observed. The effect was found to be related to a sizable contamination of ν_e^{cc} in the $\bar{\nu}$ beam from cascade decays of defocused $\pi^+ \rightarrow \mu^+ \rightarrow e^+ \nu_e \bar{\nu}_\mu$. The same behavior is not as evident in the ν running driven region ($\delta_{CP} > \pi$) due to the combined effect of the reduced cross section of $\bar{\nu}_e$ and the fact that π^- are less abundantly produced than π^+. This consideration motivated a reoptimization of the horn shape in view of using a graphite target taking into account in particularly the need for a reduced contamination from wrong–charge π.

---

[7]FLUKA 2002.4 was used in previous studies

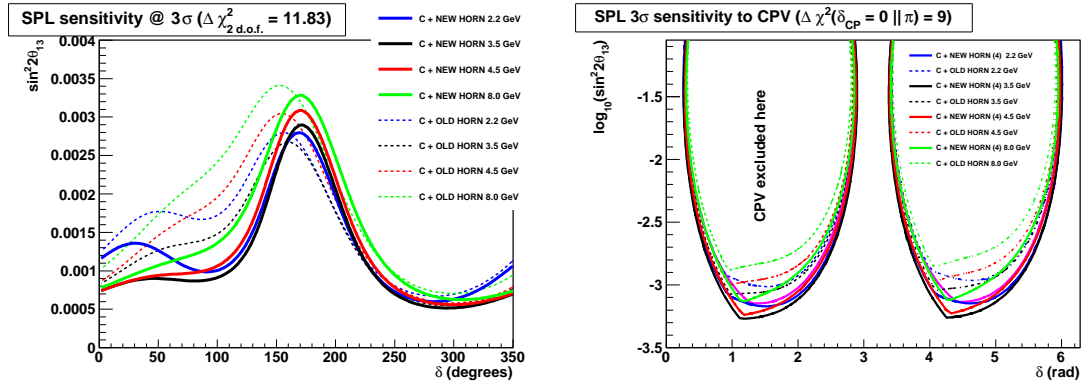|	+ focusing	- focusing
ν_μ (%)	88.9 → **95.6**	26.1 → **11.2**
$\bar{\nu}_\mu$ (%)	10.5 → **3.9**	73.4 → **88.4**
ν_e (%)	0.60 → **0.56**	0.17 → **0.09**
$\bar{\nu}_e$ (%)	0.052 → **0.025**	0.340 → **0.352**

Table 3: Standard horn → **test horn**.

The horn optimization has been performed after a full rewriting of the simulation from GEANT3 [89] to GEANT4 in order to easily change the geometrical parameters and have a quick feed-back. Two horn geometries have been implemented in GEANT4: the standard one reproducing the existing CERN prototype and a more general one based on a parametric model inspired by the shape of the MiniBOONE horn. In order to debug and validate the new GEANT4–based software, a comparison has been done with the fluxes obtained with GEANT3 using the standard horn geometry and the graphite target. Good agreement has been achieved. The parametric model is flexible enough to reproduce also the standard conical geometry with an appropriate choice of the parameters. This possibility has also been used to cross check the parametric model by comparison with the standard horn geometry.

A subset of the nine available geometrical parameters were sampled uniformly. The horn currents and the horn+reflector structure for the moment were maintained as in the original design. The resulting fluxes were analyzed and ranked according to the requirement of having low enough "wrong-CP" neutrino contamination and high flux for the signal component. More sophisticated selection techniques (i.e. based on final sensitivity on physical parameters and energy spectrum shape) and further tuning would be possible but has not yet been fully pursued. One of the horn shapes selected with the outlined heuristic procedure has been studied in more detail (will be denoted as "test horn" in the following). The most evident modifications with respect to the previous design are the presence of a forward "end-cap" in the horn (effective in removing low–angle wrong–sign pions) and the thickness of the reflector which is larger by ~ 10 cm. The radius of the inner conductor is as in the previous design (3.7 cm). With the test horn the ν_μ and ν_e energy spectra are shifted to higher energies with an increase in statistics particularly around 5-600 MeV. The wrong-CP component on the other hand is reduced by more than a factor two. The beam composition for the standard and test horn is detailed in Tab.3 for positive and negative focusing.

Profiting of the relative horn ($r = 0.5$ m) and tunnel ($L = 40$ m, $r = 2$ m) compactness the idea of using a battery of four horns in parallel has been proposed. This arrangement would imply reduced stress on the targets via lower frequency (12.5 Hz) or lower proton flux depending on the injection strategy. This choice would bring the incoming beam power in the regime which is currently considered as a viable upper limit for solid targets operations (~ 1 MW). This scenario has been implemented and tested with the GEANT4 simulation. Small flux loss even up to big lateral displacements (r) are found. In the extreme case of putting the four horns at the tunnel edge ($r = r_{TUNNEL} - r_{HORN}$) the flux of ν_μ is reduced by 13% at 4.5 GeV. The baseline configuration with horns as central as possible

$(r \sim r_{HORN}\sqrt{2})$ causes an almost negligible loss of ν_μ. The presence of a magnetic field in all the horns simultaneously or in each horn separately does not change significantly the predicted fluxes.

Sensitivity limits on $\sin^2 2\theta_{13}$ calculated with GLoBES 3.0.14 are shown in Fig. 20. The performance of the MEMPHYS Water Cherenkov detector [92] at the level of physics performance (efficiencies, background rejection, etc.) is implemented in the AEDL file `SPL.glb` which is distributed with GLoBES [78]. A mass of 0.44 Mton and a data taking of 8+2 years $\bar{\nu}+\nu$-running has been assumed. The dashed curves refer to the standard horn design in combination with the graphite target while the continuous ones refer to the test horn. A significant improvement is observed in the $\bar{\nu}$ running driven region as wanted. The graphite limits after the horn upgrade are in general even more performing than those obtained with the standard liquid mercury design. It must be noted that this result is still to be considered as preliminary since the NC-π^0 background has not yet been corrected for the change in the neutrino energy spectrum. This correction anyway will not alter the conclusions of this study since the bulk of the background is coming from the intrinsic $\nu_e+\bar{\nu}_e$ beam contamination which has been exactly taken into account. Increasing the background by 30% induces a worsening in the limit which is $< 1\cdot10^{-4}$ (mainly in the $\bar{\nu}$ driven δ region). The CP violation discovery potential is shown in Fig.20. Parameter regions for which a $\Delta\chi^2 > 9$ is obtained when fitting under the CP conserving hypotheses ($\delta_{CP} = 0, \pi$) allow the CPV discovery at more than 3σ. Also in this case a sizable improvement is obtained (lowest $\sin^2 2\theta_{13}$ passes from $\sim 8\cdot10^{-4}$ to $\sim 5\cdot10^{-4}$). It can be noticed than in general the 3.5 GeV and 4.5 GeV energies are still the preferred ones also within the test focusing.
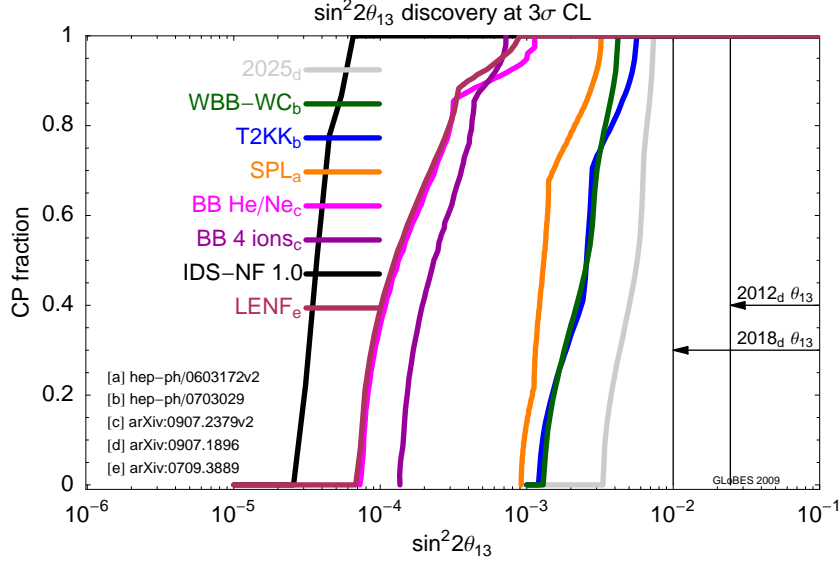

Figure 20: 3σ sensitivity to $\sin^2 2\theta_{13}$. The standard and the test horn both with a graphite target are compared. 3σ CP violation discovery. Taken from Ref. [13].
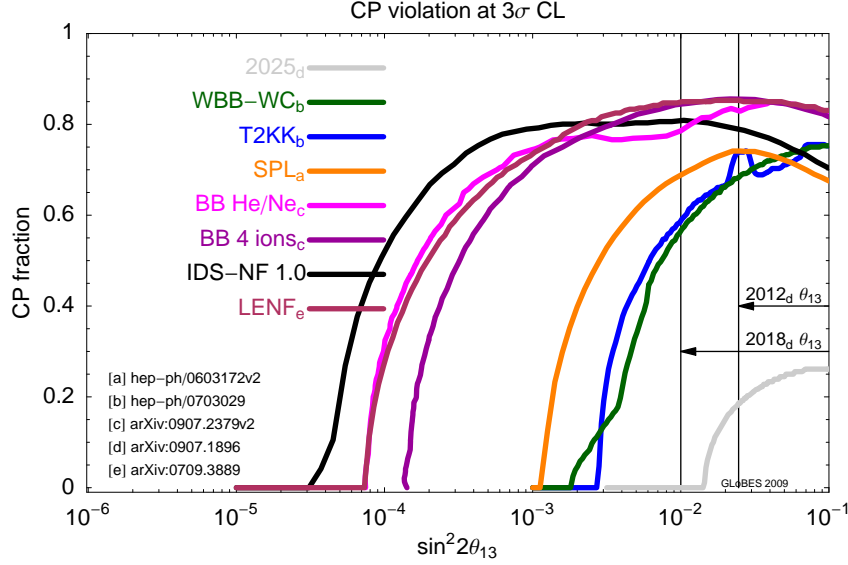
In summary the possibility to use a solid target looks very appealing for the SPL-Fréjus Super Beam. Further steps which are foreseen include the use of the HARP experiment "thick target" data to put the results on pion yields in graphite on a stronger experimental basis.
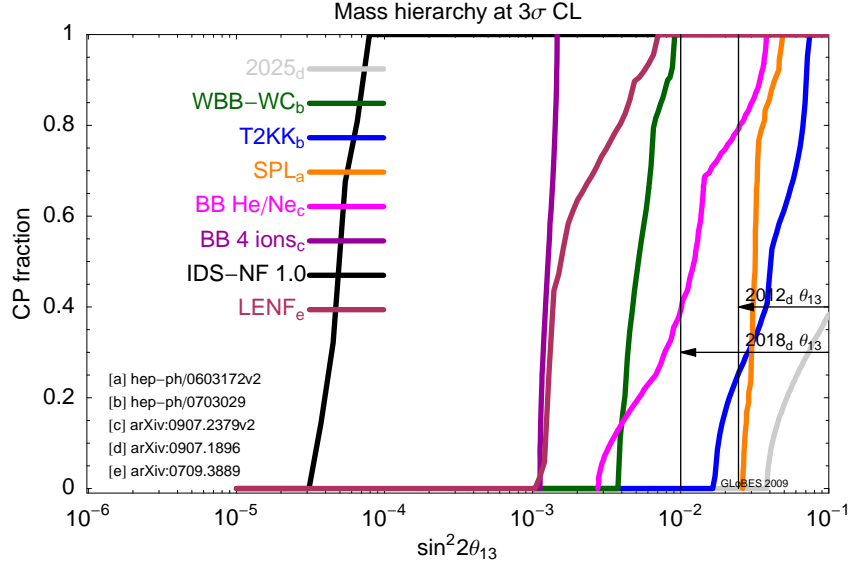
7   Updated comparison

In Figs. 21-23 we present the comparison of the updated setups for the SPL superbeam, beta-beams and Nufact. The curves correspond to 3σCL (1 dof) and the known parameters have been fixed to $\Delta m_{31}^2 = 0.0024 \text{eV}^2$, $\Delta m_{21}^2 = 8 \times 10^{-5}$ eV^2 and $\theta_{23} = 45°$.

Figure 21: Update of the comparison of the physics reach of different future facilities in $\sin^2 2\theta_{13}$. Prepared by P. Huber for this EURONU report using the GLoBES package [24,25]. Curves are taken from [a] [78], [b] [93] , [c] [10], [d] [2] and [e] [48].

Figure 22: Update of the comparison of the physics reach of different future facilities in leptonic CP violation. Prepared by P. Huber for this EURONU report using the GLoBES package [24, 25]. Curves are taken from [a] [78], [b] [93] , [c] [10], [d] [2] and [e] [48].

Figure 23: Update of the comparison of the physics reach of different future facilities in the neutrino mass hierarchy. Prepared by P. Huber for this EURONU report using the GLoBES package [24, 25]. Curves are taken from [a] [78], [b] [93] , [c] [10], [d] [2] and [e] [48].

References

[1] A. Bandyopadhyay et al. Physics at a future Neutrino Factory and super-beam facility. *Rept. Prog. Phys.*, 72:106201, 2009.

[2] Patrick Huber, Manfred Lindner, Thomas Schwetz, and Walter Winter. First hint for CP violation in neutrino oscillations from upcoming superbeam and reactor experiments. *JHEP*, 11:044, 2009.

[3] Mattias Blennow and Enrique Fernandez-Martinez. Neutrino oscillation parameter sampling with MonteCUBES. *Comput. Phys. Commun.*, 181:227–231, 2010.

[4] Andrea Donini, Ken-ichi Fuki, J. Lopez-Pavon, Davide Meloni, and Osamu Yasuda. The discovery channel at the Neutrino Factory: $\nu_\mu \to \nu_\tau$ pointing to sterile neutrinos. *JHEP*, 08:041, 2009.

[5] Joachim Kopp, Toshihiko Ota, and Walter Winter. Neutrino factory optimization for non-standard interactions. *Phys. Rev.*, D78:053007, 2008.

[6] Stefan Antusch, Mattias Blennow, Enrique Fernandez-Martinez, and Jacobo Lopez-Pavon. Probing non-unitary mixing and CP-violation at a Neutrino Factory. *Phys. Rev.*, D80:033002, 2009.

[7] A. Donini and J. Kopp. Should a ν_τ detector be included in the neutrino factory baseline setup? `Internal note for IDS-NF collaboration, Physics Performance Evaluation Group (PPEG)`, 2009.

[8] Jian Tang and Walter Winter. Physics with near detectors at a neutrino factory. *Phys. Rev.*, D80:053001, 2009.

[9] Enrique Fernandez-Martinez. The gamma = 100 Beta-Beam revisited. *0912.3804*, 2009.

[10] Sandhya Choubey, Pilar Coloma, Andrea Donini, and Enrique Fernandez-Martinez. Optimized Two-Baseline Beta-Beam Experiment. *JHEP*, 12:020, 2009.

[11] Mats Lindroos, Bob McElrath, Christopher Orme, and Thomas Schwetz. Measuring neutrino mass with radioactive ions in a storage ring. *Eur. Phys. J.*, C64:549–560, 2009.

[12] Jose Bernabeu, Catalina Espinoza, Christopher Orme, Sergio Palomares-Ruiz, and Silva Pascoli. A combined beta-beam and electron capture neutrino experiment. *JHEP*, 06:040, 2009.

[13] A. Longhin. Study of the performance of the SPL-Fréjus Super Beam using a graphite target. `EURONU note EURONU-WP2-01, May 2009`, 2009.

[14] F. Ardellier et al. Letter of intent for Double-CHOOZ: A search for the mixing angle theta(13). *hep-ex/0405032*, 2004.

[15] Xinheng Guo et al. A precision measurement of the neutrino mixing angle theta(13) using reactor antineutrinos at Daya Bay. *hep-ex/0701029*, 2007.

[16] Soo-Bong Kim. RENO: Reactor experiment for neutrino oscillation at Yonggwang. *AIP Conf. Proc.*, 981:205–207, 2008.

[17] Y. Itow et al. The jhf-kamioka neutrino project. *Nucl. Phys. Proc. Suppl.*, 111:146–151, 2001.

[18] I. Ambats et al. Nova proposal to build a 30-kiloton off-axis detector to study neutrino oscillations in the fermilab numi beamline. *hep-ex/0503053*, 2004.

[19] H. Minakata, H. Sugiyama, O. Yasuda, K. Inoue, and F. Suekane. Reactor measurement of theta(13) and its complementarity to long-baseline experiments. *Phys. Rev.*, D68:033017, 2003.

[20] Patrick Huber, M. Lindner, and W. Winter. Synergies between the first-generation JHF-SK and NuMI superbeam experiments. *Nucl. Phys.*, B654:3–29, 2003.

[21] Patrick Huber, M. Lindner, T. Schwetz, and W. Winter. Reactor neutrino experiments compared to superbeams. *Nucl. Phys.*, B665:487–519, 2003.

[22] P. Huber, M. Lindner, M. Rolinec, T. Schwetz, and W. Winter. Prospects of accelerator and reactor neutrino oscillation experiments for the coming ten years. *Phys. Rev.*, D70:073014, 2004.

[23] Kendall B. McConnel and Michael H. Shaevitz. Comparisons and combinations of reactor and long-baseline neutrino oscillation measurements. *Int. J. Mod. Phys.*, A21:3825–3844, 2006.

[24] Patrick Huber, M. Lindner, and W. Winter. Simulation of long-baseline neutrino oscillation experiments with GLoBES. *Comput. Phys. Commun.*, 167:195, 2005. `http://www.mpi-hd.mpg.de/lin/globes/`.

[25] Patrick Huber, Joachim Kopp, Manfred Lindner, Mark Rolinec, and Walter Winter. New features in the simulation of neutrino oscillation experiments with GLoBES 3.0. *Comput. Phys. Commun.*, 177:432–438, 2007.

[26] Thomas Schwetz, Mariam Tortola, and Jose W. F. Valle. Three-flavour neutrino oscillation update. *New J. Phys.*, 10:113011, 2008.

[27] M. McFarlane, K. Heeger, P. Huber, C. Lewis, and W. Wang. Study of the Sensitivity of the Daya Bay Reactor Neutrino Experiment to $\sin^2 2\theta_{13}$ using GLoBES. 2009. In preparation.

[28] K. Hasegawa. The j-parc neutrino beam. Talk given at NNN 08, Paris France, `http://nnn08.in2p3.fr/` .

[29] Resource-loaded schedule. Director's Preliminary Cost and Schedule Review, March 16-17, 2009, `http://projectx.fnal.gov`.

[30] Walter Winter. Understanding CP phase-dependent measurements at neutrino super-beams in terms of bi-rate graphs. *Phys. Rev.*, D70:033006, 2004.

[31] Mattias Blennow and Enrique Fernandez-Martinez. MonteCUBES homepage. `http://wwwth.mppmu.mpg.de/members/blennow/montecubes/`.

[32] Andrew Gelman and Donald B. Rubin. Inference from Iterative Simulation Using Multiple Sequences. *Statist. Sci.*, 7:457–472, 1992.

[33] Gary J. Feldman and Robert D. Cousins. A Unified Approach to the Classical Statistical Analysis of Small Signals. *Phys. Rev.*, D57:3873–3889, 1998.

[34] C. Athanassopoulos et al. Evidence for anti-nu/mu –¿ anti-nu/e oscillation from the LSND experiment at the Los Alamos Meson Physics Facility. *Phys. Rev. Lett.*, 77:3082–3085, 1996.

[35] A. A. Aguilar-Arevalo et al. A Search for electron neutrino appearance at the $\Delta m^2 \sim$ 1eV^2 scale. *Phys. Rev. Lett.*, 98:231801, 2007.

[36] A. Donini, M. B. Gavela, P. Hernandez, and S. Rigolin. Neutrino mixing and CP-violation. *Nucl. Phys.*, B574:23–42, 2000.

[37] A. Donini and D. Meloni. The 2+2 and 3+1 four-family neutrino mixing at the neutrino factory. *Eur. Phys. J.*, C22:179–186, 2001.

[38] A. Donini, Maurizio Lusignoli, and D. Meloni. Telling three from four neutrinos at the neutrino factory. *Nucl. Phys.*, B624:405–422, 2002.

[39] A. Donini, M. Maltoni, D. Meloni, P. Migliozzi, and F. Terranova. 3+1 sterile neutrinos at the CNGS. *JHEP*, 12:013, 2007.

[40] T. Abe et al. Detectors and flux instrumentation for future neutrino facilities. *JINST*, 4:T05001, 2009.

[41] A. M. Dziewonski and D. L. Anderson. Preliminary reference earth model. *Phys. Earth Planet. Interiors*, 25:297–356, 1981.

[42] S.V. Panasyuk. Reference earth model (rem) webpage. `http://cfauves5.harvard.edu/lana/rem/index.html`.

[43] Carla Biggio, Mattias Blennow, and Enrique Fernandez-Martinez. Loop bounds on non-standard neutrino interactions. *JHEP*, 03:139, 2009.

[44] Carla Biggio, Mattias Blennow, and Enrique Fernandez-Martinez. General bounds on non-standard neutrino interactions. *JHEP*, 08:090, 2009.

[45] IDS-NF. International design study for the neutrino factory. Website: `http:www.ids-nf.org`.

[46] N. C. Ribeiro, H. Minakata, H. Nunokawa, S. Uchinami, and R. Zukanovich-Funchal. Probing Non-Standard Neutrino Interactions with Neutrino Factories. *JHEP*, 12:002, 2007.

[47] Steve Geer, Olga Mena, and Silvia Pascoli. A Low energy neutrino factory for large θ_{13}. *Phys. Rev.*, D75:093001, 2007.

[48] Alan D. Bross, Malcolm Ellis, Steve Geer, Olga Mena, and Silvia Pascoli. A Neutrino factory for both large and small θ_{13}. *Phys. Rev.*, D77:093012, 2008.

[49] Zurab Berezhiani and Anna Rossi. Limits on the non-standard interactions of neutrinos from e+ e- colliders. *Phys. Lett.*, B535:207–218, 2002.

[50] S. Davidson, C. Pena-Garay, N. Rius, and A. Santamaria. Present and future bounds on non-standard neutrino interactions. *JHEP*, 03:011, 2003.

[51] Stefan Antusch, Jochen P. Baumann, and Enrique Fernandez-Martinez. Non-Standard Neutrino Interactions with Matter from Physics Beyond the Standard Model. *Nucl. Phys.*, B810:369–388, 2009.

[52] M. B. Gavela, D. Hernandez, T. Ota, and W. Winter. Large gauge invariant non-standard neutrino interactions. *Phys. Rev.*, D79:013007, 2009.

[53] S. Antusch, C. Biggio, E. Fernandez-Martinez, M. B. Gavela, and J. Lopez-Pavon. Unitarity of the Leptonic Mixing Matrix. *JHEP*, 10:084, 2006.

[54] A. Abada, C. Biggio, F. Bonnet, M. B. Gavela, and T. Hambye. Low energy effects of neutrino masses. *JHEP*, 12:061, 2007.

[55] S. Geer. Neutrino beams from muon storage rings: Characteristics and physics potential. *Phys. Rev.*, D57:6989–6997, 1998.

[56] A. De Rujula, M. B. Gavela, and P. Hernandez. Neutrino oscillation physics with a neutrino factory. *Nucl. Phys.*, B547:21–38, 1999.

[57] A. Donini, D. Meloni, and P. Migliozzi. The silver channel at the Neutrino Factory. *Nucl. Phys.*, B646:321–349, 2002.

[58] D. Autiero et al. The synergy of the golden and silver channels at the Neutrino Factory. *Eur. Phys. J.*, C33:243–260, 2004.

[59] J. Burguet-Castell, M. B. Gavela, J. J. Gomez-Cadenas, P. Hernandez, and Olga Mena. On the measurement of leptonic CP violation. *Nucl. Phys.*, B608:301–318, 2001.

[60] Patrick Huber and Walter Winter. Neutrino factories and the 'magic' baseline. *Phys. Rev.*, D68:037301, 2003.

[61] A. Cervera et al. Golden measurements at a neutrino factory. *Nucl. Phys.*, B579:17–55, 2000.

[62] E. Fernandez-Martinez, M. B. Gavela, J. Lopez-Pavon, and O. Yasuda. CP-violation from non-unitary leptonic mixing. *Phys. Lett.*, B649:427–435, 2007.

[63] P. Huber, M. Lindner, M. Rolinec, and W. Winter. Optimization of a neutrino factory oscillation experiment. *Phys. Rev.*, D74:073003, 2006.

[64] Davide Meloni. Solving the octant degeneracy with the Silver channel. *Phys. Lett.*, B664:279–284, 2008.

[65] A. Donini, E. Fernandez-Martinez, D. Meloni, and S. Rigolin. nu/mu disappearance at the SPL, T2K-I, NOnuA and the neutrino factory. *Nucl. Phys.*, B743:41–73, 2006.

[66] V. Barger, S. Geer, and K. Whisnant. Neutral currents and tests of three-neutrino unitarity in long-baseline experiments. *New J. Phys.*, 6:135, 2004.

[67] A. Bueno, Mario Campanelli, and A. Rubbia. Physics potential at a neutrino factory: Can we benefit from more than just detecting muons? *Nucl. Phys.*, B589:577–608, 2000.

[68] Joachim Kopp, Manfred Lindner, Toshihiko Ota, and Joe Sato. Non-standard neutrino interactions in reactor and superbeam experiments. *Phys. Rev.*, D77:013007, 2008.

[69] Tommy Ohlsson, Thomas Schwetz, and He Zhang. Non-standard neutrino interactions in the Zee-Babu model. *Phys. Lett.*, B681:269–275, 2009.

[70] Michal Malinsky, Tommy Ohlsson, and He Zhang. Non-Standard Neutrino Interactions from a Triplet Seesaw Model. *Phys. Rev.*, D79:011301, 2009.

[71] Carlo Giunti, Marco Laveder, and Walter Winter. Short-Baseline Electron Neutrino Disappearance at a Neutrino Factory. *Phys. Rev.*, D80:073005, 2009.

[72] P. Zucchelli. A novel concept for a anti-nu/e / nu/e neutrino factory: The beta beam. *Phys. Lett.*, B532:166–172, 2002.

[73] J. Burguet-Castell, D. Casper, J. J. Gomez-Cadenas, P. Hernandez, and F. Sanchez. Neutrino oscillation physics with a higher gamma beta- beam. *Nucl. Phys.*, B695:217–240, 2004.

[74] J. Burguet-Castell, D. Casper, E. Couce, J. J. Gomez-Cadenas, and P. Hernandez. Optimal beta-beam at the CERN-SPS. *Nucl. Phys.*, B725:306–326, 2005.

[75] C. Rubbia, A. Ferrari, Y. Kadi, and V. Vlachoudis. Beam cooling with ionisation losses. *Nucl. Instrum. Meth.*, A568:475–487, 2006.

[76] A. Donini and E. Fernandez-Martinez. Alternating ions in a beta-beam to solve degeneracies. *Phys. Lett.*, B641:432–439, 2006.

[77] Carlo Rubbia. Ionization cooled ultra pure beta-beams for long distance $\nu_e \to \nu_\mu$ transitions, θ_{13} phase and CP- violation. *hep-ph/0609235*, 2006.

[78] Jean-Eric Campagne, M. Maltoni, M. Mezzetto, and T. Schwetz. Physics potential of the CERN-MEMPHYS neutrino oscillation project. *JHEP*, 04:003, 2007.

[79] M. Sajjad Athar et al. India-based Neutrino Observatory: Project Report. VolumeI. A Report of the INO Feasibility Study. Updated from the earlier Interim Report of May 1, 2005., 2006.

[80] Andrea Donini and Mats Lindroos. Optimisation of a beta beam. Presented at 10th International Workshop on Neutrino Factories, Superbeams and Betabeams: Nufact08, Valencia, Spain, 30 Jun - 5 Jul 2008, 2008.

[81] P. I. Krastev and S. T. Petcov. Resonance Amplification and t Violation Effects in Three Neutrino Oscillations in the Earth. *Phys. Lett.*, B205:84–92, 1988.

[82] Jiro Arafune, Masafumi Koike, and Joe Sato. CP violation and matter effect in long baseline neutrino oscillation experiments. *Phys. Rev.*, D56:3093–3099, 1997.

[83] J. Bernabeu. CP, T violation in neutrino oscillations. *hep-ph/9904474*, 1999.

[84] K. Dick, M. Freund, M. Lindner, and A. Romanino. CP-violation in neutrino oscillations. *Nucl. Phys.*, B562:29–56, 1999.

[85] J. Bernabeu and M. C. Banuls. CP and T violation in neutrino oscillations. *Nucl. Phys. Proc. Suppl.*, 87:315–317, 2000.

[86] Evgeny Khakimovich Akhmedov, Robert Johansson, Manfred Lindner, Tommy Ohlsson, and Thomas Schwetz. Series expansions for three-flavor neutrino oscillation probabilities in matter. *JHEP*, 04:078, 2004.

[87] Joe Sato. Monoenergetic neutrino beam for long baseline experiments. *Phys. Rev. Lett.*, 95:131804, 2005.

[88] J. Bernabeu, J. Burguet-Castell, C. Espinoza, and M. Lindroos. Monochromatic neutrino beams. *JHEP*, 12:014, 2005.

[89] Jean Eric Campagne and Antoine Cazes. The theta(13) and delta(CP) sensitivities of the SPL- Frejus project revisited. *Eur. Phys. J.*, C45:643–657, 2006.

[90] I. Efthymiopoulos. MERIT- The high intensity liquid mercury target experiment at the CERN PS. `Nuclear Science Symposium Conference Record, IEEE 19-25 Oct. 2008, 3302-3305.`, 2008.

[91] Study of the performance of the SPL-Fréjus Super Beam using a graphite target. http://indico.in2p3.fr/categoryDisplay.py?categId=203, 2009.

[92] A. de Bellefon et al. MEMPHYS: A large scale water Cherenkov detector at Fréjus. `hep-ex/0607026`, 2006.

[93] V. Barger, P. Huber, D. Marfatia, and W. Winter. Which long-baseline neutrino experiments are preferable? *Phys. Rev.*, D76:053005, 2007.